SAL 2002- 1

A Meshfree Method for Incompressible Fluid Dynamics Problems

I. Tsukanov, V. Shapiro, S. Zhang

A Meshfree Method for Incompressible Fluid Dynamics Problems

I.Tsukanov[a] *, V.Shapiro[a], S.Zhang[b]
[a]Spatial Automation Laboratory
University of Wisconsin-Madison
1513 University Avenue
Madison, WI 53706, U.S.A.

[b]General Motors R&D Center
Warren, MI 48090, U.S.A.

Accepted for publication in Int. Journal for Numerical Methods in Engineering

Abstract

We show that meshfree variational methods may be utilized for solution of incompressible fluid dynamics problems using the R-function method (RFM). The proposed approach constructs an approximate solution that satisfies all prescribed boundary conditions exactly using approximate distance fields for portions of the boundary, transfinite interpolation, and computations on a non-conforming spatial grid. We give detailed implementation of the method for two common formulations of the incompressible fluid dynamics problem: first using scalar stream function formulation and then using vector formulation of the Navier-Stokes problem with artificial compressibility approach. Extensive numerical comparisons with commercial solvers and experimental data for the benchmark back-facing step channel problem reveal strengths and weaknesses of the proposed meshfree method.

Keywords: meshfree method, distance field, solution structure, Navier-Stokes problem, stream function, artificial compressibility approach

1 Introduction

1.1 Towards meshfree solution of computational fluid dynamics problems

Modeling of the incompressible fluid flow involves solution of the Navier-Stokes equations inside a geometric domain. The interaction between the fluid and the boundary of the geometric domain, in terms of the mathematical model is described by boundary conditions, formulated for viscous fluid as known velocity profile at the inlet and zero velocity at the walls. The nature of this problem makes its treatment difficult: the solution algorithm needs to incorporate two distinct types of information — (1) analytical information that describes the Navier-Stokes equations and functions given as boundary conditions; and (2) geometric information about boundaries where the boundary conditions are prescribed. Conventional methods of engineering analysis solve this problem by employing first, the spatial discretization of the geometric domain (a mesh that conforms to the boundary of the geometric domain), and second, the discretization of the Navier-Stokes equations and the boundary conditions over the discretized geometry domain. The resulting approximation, therefore, unifies both functional and geometric information. Such approach, despite its wide usage, has some drawbacks. For example, it is well known that the construction of a "good" mesh is a difficult and time consuming task. In engineering practice design iterations require efficient feedback from the analysis results to the geometric model. However, employment of conforming meshes for solution of engineering problems is not quite suitable for design purposes, because the spatial grid restricts changes of the parameters of the geometric model such that it is difficult or even impossible to change the shape of the model without remeshing.

*Corresponding author. E-mail: igor@sal-cnc.me.wisc.edu

These difficulties in the conventional approaches led to the development of methods which use non-conforming [1] meshes or no meshes at all. These new meshfree (sometimes they are also called *meshless*) methods represent a solution of the problem by linear combination of basis functions which may be constructed over meshes not conforming to the shape of the geometric model [3, 23, 4, 17, 8, 21, 25, 18, 7, 9]. However, the employment of non-conforming spatial discretization makes the treatment of boundary conditions more difficult. Proposed remedies include the combination of Element Free Galerkin Method (EFG) [4] with finite element shape functions near the boundary [17], the use of modified variational principle [20], window or correction functions that vanish on the boundary [9], and Lagrange multipliers. Although these techniques appear promising, they often contradict the meshfree nature of the approximation near the boundary, introduce additional constraints on solutions, or lead to systems with an increased number of unknowns [13]. Several promising transformation-based approaches to satisfying essential boundary conditions at desired nodal locations have been recently proposed and compared by J.-S. Chen [8].

The meshing problem can be substantially simplified by employment of the Cartesian grid methods [42, 1, 11, 5]. These methods represent the geometric model by a hierarchical set of cubical/rectangular cells that simplify computation of the partial derivatives using a finite difference scheme. Instead of requiring that cells conform to the boundaries of the domain, the geometric model of the domain is approximated by quad/octtree spatial decompositions to any prescribed accuracy. This approach is accompanied by introduction of additional sources of errors and potentially exponential (in the subdivision depth) increase in computational cost.

In contrast to Cartesian grid methods, immersed boundary methods [24, 14, 15] solve the problem using a uniform non-conforming grid of points that cover the geometric model. Influence of the boundaries and boundary conditions is accounted for by modification of the differential equation of the problem, based on special case analysis.

In this paper, we describe a method that also relies on a non-conforming uniform rectangular grid, but goes substantially further. All prescribed boundary conditions are satisfied *exactly* by transfinitely interpolating individual boundary conditions inversely proportional to the approximate distance to each boundary portion. The technique can be applied systematically to any and all boundary value problems using the theory of R-functions [30], and the resulting interpolant can be combined with just about any standard numerical solution method. The method is demonstrated with variational methods applied to the solution of incompressible fluid dynamics problems: first using scalar stream function formulation, and then using vector formulation of the Navier-Stokes problem with artificial compressibility approach.

1.2 Brief History of the Method

Kantorovich showed that Dirichlet boundary conditions could be satisfied exactly using functions vanishing on the boundary of a geometric object [16]. He proposed to represent a solution satisfying Dirichlet boundary condition $u_{|\partial\Omega} = \varphi$ in the following form:

$$u = \omega \sum_{i=1}^{N} C_i \chi_i + \varphi, \tag{1}$$

where ω is a function taking on zero value on the boundary of the domain; $\{\chi_i\}_{i=1}^{N}$ is a system of linearly independent basis functions; $\{C_i\}_{i=1}^{N}$ is a vector of unknown coefficients and φ is a function given as a boundary condition. Different sets of the coefficients $\{C_i\}_{i=1}^{N}$ give different functions u but all of them satisfy the prescribed boundary condition. Numerical values of the unknown coefficients can be obtained via variational or projectional methods. Application of Kantorovich's method was limited to very simple geometric domains, because at that time it was unclear how to construct function ω for arbitrary geometric domains.

Several years later, Rvachev proposed that functions taking on zero value on the boundary of a geometric domain can be constructed for virtually any geometric object using R-functions [27, 28, 34]. Informally, R-functions serve as a construction toolkit transforming a set-theoretic description of the boundary of a geometric object into a real valued function whose zero set coincides with the boundary. Detailed discussion on R-functions and construction techniques is outside of the scope of this paper, but it can be found in numerous references [28, 34, 35, 26, 29] and will be illustrated in section 2.2. Functions constructed using R-functions are differentiable everywhere except a finite number of points [28, 35] and behave as distances to the boundaries near the boundary points. We will refer

[1] This should not be confused with the another commonly used terminology of "conforming/non-conforming finite element". In this paper the non-conformance of the spatial grid to the shape of the geometric domain means that the grid is extended beyond, and unconstrained by the boundary of the geometric domain.

to such functions as approximate distance fields. Besides techniques based on the theory of R-functions [28], other methods may also be applied for construction of approximate distance fields. For example, the level set method [33, 32] results in a distance-like functions, albeit defined at a discrete set of points and usually implicitly. In contrast, the approximate distance fields constructed using R-functions are explicitly defined at all points of the space. The successful employment of the level set method to model holes and inclusions was discussed in [38]. Similar technique was used to model crack development and propagation in [37].

Approximate distance fields can be used for interpolation of the functions and their derivatives prescribed on the boundary pieces of a geometric object [31]. Representation of boundaries of a geometric object by approximate distance fields made possible the extension of the Kantorovich's method into the R-function method (RFM). The RFM allows the satisfaction of many types of boundary conditions exactly by employing *solution structures* that incorporate boundary conditions, approximate distance fields, and basis functions with unknown coefficients [30]. RFM is essentially a meshfree method because it places no restriction on the choice of the basis functions: they can be constructed over conforming or non-conforming mesh. For example, finite elements can be used as basis functions; in this case, RFM can be viewed as an enhanced finite element method that treats all given boundary conditions exactly. But in this paper, all computations were performed over a uniform rectangular grid of B-splines and performed within the SAGE system developed by authors [41]. In [36], we showed that the method is particularly effective in dealing with moving and deforming boundary conditions.

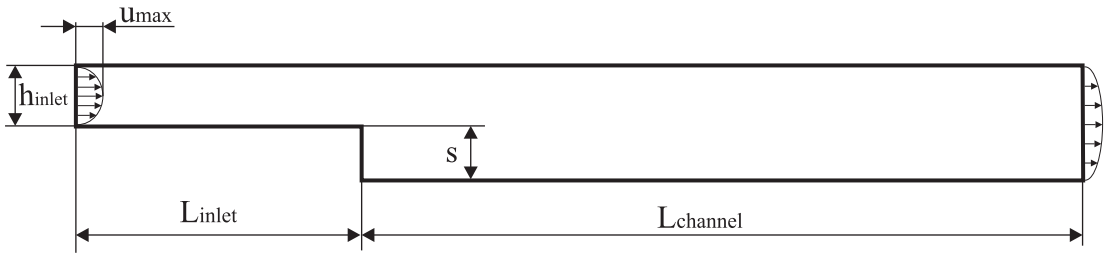

Figure 1: Parametrization of the geometry of a back facing step channel

1.3 Scope and outline

This paper serves two purposes. First, the application of the RFM to Computational Fluid Dynamics (CFD) is illustrated through two different formulations; second, the numerical properties (accuracy and convergence) of the RFM, applied to these formulations, are investigated. The paper will show that the RFM approach to CFD provides a unique and flexible method to link both the functional and geometric information in a unified manner. It will also be shown that the artificial compressibility approach gives good results for low Reynolds number flow ($Re < 400$). For higher Reynolds numbers flows the RFM needs to be implemented either with Finite Volume (FV)/Finite Difference (FD) numerical schemes or using the regularization approach described in [10].

Throughout the paper, we assume that flow is laminar, fluid is Newtonian, and we focus on two-dimensional problems. In this case incompressible two dimensional viscous flow is described by Navier-Stokes equations and the continuity equation [19]:

$$\begin{aligned} u\frac{\partial u}{\partial x} + v\frac{\partial u}{\partial y} - \frac{1}{Re}\nabla^2 u &= -Eu\frac{\partial p}{\partial x}; \\ u\frac{\partial v}{\partial x} + v\frac{\partial v}{\partial y} - \frac{1}{Re}\nabla^2 v &= -Eu\frac{\partial p}{\partial y} \\ \frac{\partial u}{\partial x} + \frac{\partial v}{\partial y} &= 0, \end{aligned} \tag{2}$$

where variables u and v are the velocity components in the x and y coordinate directions respectively, p is the pressure variable, $Re = \frac{2}{3}u_{max}\frac{2h_{\text{inlet}}}{\nu}$ and $Eu = \frac{P}{\rho u_{max}^2}$ are Reynolds and Euler numbers respectively. We explore

the accuracy of the RFM and its convergence properties, solving a standard textbook benchmark problem: an incompressible viscous fluid flow in a two-dimensional back-facing step channel, whose parametrization is shown in Figure 1. For this problem experimental data [2], as well as the computer simulation results given by the conventional fluid dynamics systems, are available. For concreteness we let the geometric parameters take on the following numerical values: $L_{\text{inlet}} = 5$, $L_{\text{channel}} = 12$, $h_{\text{inlet}} = 0.5$ and $s = 0.471$. In order to simplify the comparison of the RFM modeling results with experimental data, we use the same ratio between h_{inlet} and s as in [2]. Boundary conditions are formulated as a parabolic velocity profile with $u_{max} = 1.5$ at the inlet and zero velocity at the walls of the channel.

Most meshfree methods employ some variational principle in order to solve the problem, and the RFM is no exception. Since RFM treats the given boundary conditions exactly, the variational principle is applied to the differential equation(s) of the problem only. Because viscous fluid flows do not conserve energy, we employ a least squares method. In the paper we discuss the application of the RFM to two different formulation of the incompressible fluid dynamics problem: stream function and artificial compressibility formulations.

The stream function formulation discussed in Section 2 substantially simplifies the initial problem reducing the system of the Navier-Stokes and continuity equations to a single equation. We use the stream function formulation as an introductory example in order to explain the concept of the RFM solution structure and the RFM solution procedure. The velocity profiles given by the RFM are in good agreement with the experimental data for Reynolds number 100. For higher Reynolds numbers the RFM overestimates the position of the reattachment point.

The accuracy of the modeling results can be improved by applying the RFM to the primitive variables of the Navier-Stokes equations via an artificial compressibility approach, detailed in Section 3. In contrast to the stream function formulation, the artificial compressibility formulation allows modeling of fluid flows in channels with arbitrary geometric shape including multiple connected channels. Further, it can be easily extended to model three-dimensional and turbulent flows. Since the artificial compressibility formulation leads to solution of a vector problem, application of the RFM to this formulation of incompressible fluid dynamics problem results in vector solution structures whose construction we explain in Section 3.2.

Section 2.5 and Section 3.4 contain the analysis of the RFM modeling results and their comparison with experimental data and numerical results obtained using the commercial fluid analysis system Fluent. Distributions of the velocity components and the pressure field given by the RFM are in good agreement with experimental data, however the employment of variational methods appears to raise some issues. These observations and possible ways to improve effectiveness of the method are discussed in Section 4.

2 RFM with stream function formulation

2.1 Stream function formulation and solution

Introduction of a stream function ψ such that $u = \frac{\partial \psi}{\partial y}$ and $v = -\frac{\partial \psi}{\partial x}$ allows us to satisfy the continuity equation and to exclude the pressure p from the momentum equations. Substitution of the stream function ψ instead of derivatives of velocity components gives a differential equation for the stream function [19]:

$$\frac{1}{Re}\nabla^4\psi - \frac{\partial \psi}{\partial y}\frac{\partial}{\partial x}\left(\nabla^2\psi\right) + \frac{\partial \psi}{\partial x}\frac{\partial}{\partial y}\left(\nabla^2\psi\right) = 0. \tag{3}$$

Boundary conditions for the stream function at the inlet can be derived from the velocity profile at the inlet which is usually known:

$$\psi_{|inlet} = \int_0^s \mathbf{V}(x,y)cos(\mathbf{n},\mathbf{V})dS, \tag{4}$$

where $\mathbf{V} = u\mathbf{i} + v\mathbf{j}$ is the velocity vector and n is the normal vector to the inlet section. Assuming a parabolic profile for the u component of the velocity vector, as shown in Figure 1, with $u_{max} = 1.5$ and $v = 0$ at the inlet, we obtain the boundary condition for stream function as:

$$\begin{aligned} &\psi_{|\text{inlet}} = \frac{2}{h_{\text{inlet}}^2}y^3 + \frac{3}{h_{\text{inlet}}}y^2; \\ &\frac{\partial \psi}{\partial n}_{|\text{inlet}} = 0. \end{aligned} \tag{5}$$

On the walls of the channel the stream function should satisfy the following boundary conditions:

$$\begin{aligned} \psi_{|\text{lower wall}} &= 0; \\ \psi_{|\text{upper wall}} &= h_{\text{inlet}}. \end{aligned} \tag{6}$$

Since we are dealing with viscous flow, velocity is assumed to be zero on all walls. This condition is expressed in terms of homogeneous Neumann boundary condition for the stream function:

$$\frac{\partial \psi}{\partial n}_{|\text{walls}} = 0. \tag{7}$$

Boundary conditions for the stream function at the outlet can be derived from two conditions: (a) the total discharge at the outlet should be the same as at the inlet, and (b) the velocity components at the outlet should respectively be: $v = 0$, and u should possess a parabolic profile as is shown in Figure 1. After simplification we get:

$$\begin{aligned} &\psi_{|\text{outlet}} = m\left(-\frac{y^3}{3} + \frac{h_{\text{inlet}} - s}{2}y^2 + h_{\text{inlet}}sy\right) + k; \\ &m = \frac{6h_{\text{inlet}}}{\left(h_{\text{inlet}} + s\right)^3}; \\ &k = \frac{m}{4}\left(3s^2 h_{\text{inlet}} + s^3\right); \\ &\frac{\partial \psi}{\partial n}_{|\text{outlet}} = 0. \end{aligned} \tag{8}$$

The geometry of the channel, equation (3) together with boundary conditions (4 – 8) constitutes a complete mathematical formulation of the problem. The first steps of solving this problem with RFM are construction of approximate distance fields for boundary pieces and the RFM solution structure for the problem. The solution structure interpolates all given boundary conditions over the specified geometry, but also includes a set of basis functions with undetermined coefficients. The subsequent solution procedure will determine the coefficients that best approximate the governing differential equation in some sense. The solution structure, as well as approximate distance fields, are usually constructed automatically without user's intervention, but below we show all the construction details manually and explicitly.

2.2 Theory of R-functions and approximate distance fields

The theory of R-functions was originally developed in Ukraine by V. L. Rvachev and his students [28, 26, 29]. A complete list of references through 2001 can be found in [22]. A brief English summary of the theory of R-functions written by Shapiro in 1988 [34] is available as a technical report.

An R-function is real-valued function whose sign is completely determined by the signs of its arguments. For example, the function xyz can be negative only when the number of its negative arguments is odd. A similar property is possessed by functions $x + y + \sqrt{xy + x^2 + y^2}$ and $xy + z + |z - yx|$, and so on. Such functions 'encode' Boolean logic functions and are called **R-functions**. Every Boolean function is a companion to infinitely many R-functions, which form a *branch* of the set of R-functions. For example, it is well known that $\min(x_1, x_2)$ is an R-function whose companion Boolean function is logical "and" ($\wedge$), and $\max(x_1, x_2)$ is an R-function whose companion Boolean function is logical "or" ($\vee$). But the same branches of R-functions contain many other functions, e.g.

$$\begin{aligned} x_1 \wedge_\alpha x_2 &\equiv \tfrac{1}{1+\alpha}\left(x_1 + x_2 - \sqrt{x_1^2 + x_2^2 - 2\alpha x_1 x_2}\right); \\ x_1 \vee_\alpha x_2 &\equiv \tfrac{1}{1+\alpha}\left(x_1 + x_2 + \sqrt{x_1^2 + x_2^2 - 2\alpha x_1 x_2}\right), \end{aligned} \tag{9}$$

where $\alpha(x_1, x_2)$ is an arbitrary symmetric function such that $-1 < \alpha(x_1, x_2) \leq 1$. The precise value of α may or may not matter, and often it can be set to a constant. For example, setting $\alpha = 1$ yields the $\min$ and $\max$ respectively, but setting $\alpha = 0$ results in much nicer functions $\vee_0$ and $\wedge_0$ that are *analytic* everywhere except when $x_1 = x_2 = 0$. Similarly, R-functions

$$x_1 \wedge_\alpha^m x_2 \equiv (x_1 \wedge_\alpha x_2)(x_1^2 + x_2^2)^{\frac{m}{2}}; \qquad x_1 \vee_\alpha^m x_2 \equiv (x_1 \vee_\alpha x_2)(x_1^2 + x_2^2)^{\frac{m}{2}} \tag{10}$$

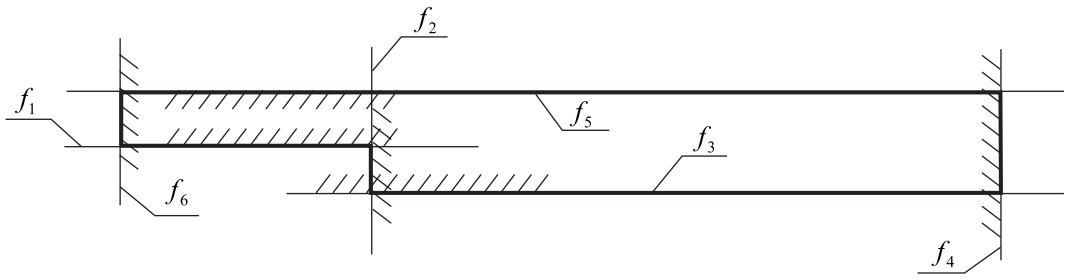

(a)

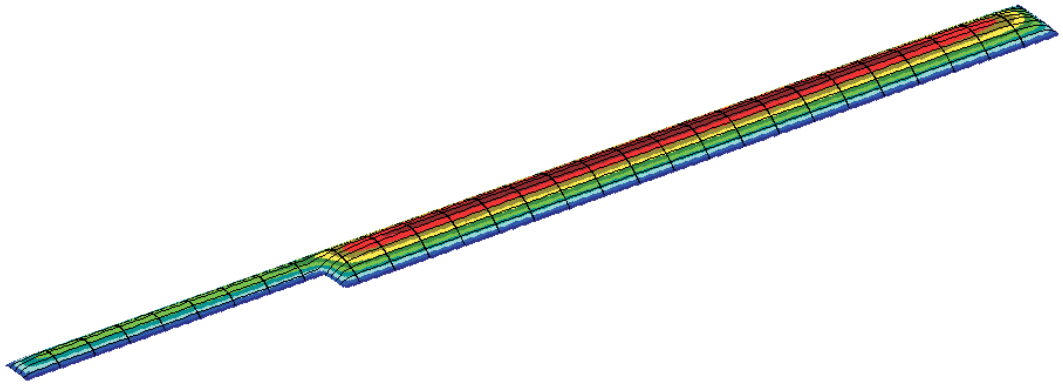

(b)

Figure 2: (a) Halfspaces that constitute a CSG representation of the channel; (b) the corresponding approximate distance field

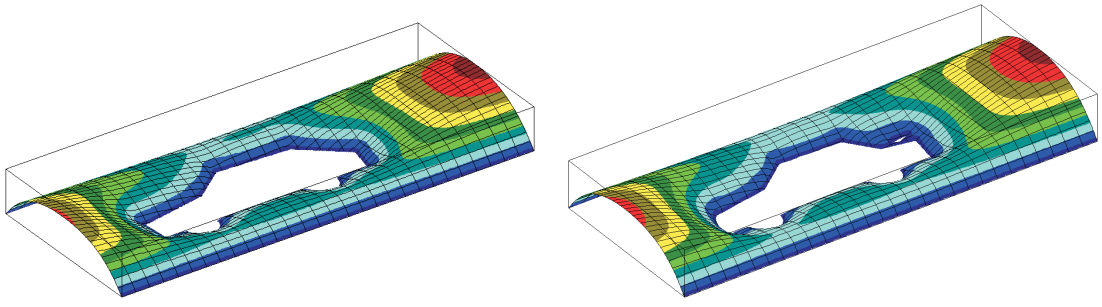

(a) (b)

Figure 3: Approximate distance fields for the portions of the boundary where non-slip boundary conditions are prescribed: (a) for the car presented in Figure 23(b); (b) for the car presented in Figure 23(c)

are analytic everywhere except the origin ($x_1 = x_2 = 0$), where they are m times differentiable. Many other systems of R-functions are studied in [28]. The choice of an appropriate system of R-functions is dictated by many considerations, including simplicity, continuity, differential properties, and computational convenience.

Just as Boolean functions, R-functions are closed under composition. Using R-functions, any object defined by a predicate on "primitive" geometric regions (e.g. regions defined by a system of inequalities) can now also be represented by a *single* inequality, or equation. The latter can be evaluated, differentiated, and possesses many other useful properties. In particular:

- the functions are constructed in a 'logical' fashion and can be controlled through intuitive user-defined parameters;
- functions can be normalized, in which case they behave as distance functions near the boundary of the object and can be differentiated everywhere [28, 35];
- functions can also be constructed for individual cells and cells complexes, given prescribed values for the functions and their gradients;
- the functions can be used to define time-varying geometry and used for modeling various complex physical phenomena.

Theory of R-functions provides the connection between logical and set operations on geometric primitives and analytic constructions. For *every* logical or set-theoretic construction, there is a corresponding approximate distance function with the above properties. Furthermore, the translation from logical and set-theoretic description is a matter of simple syntactic substitution that does not require expensive symbolic computations. For example, the geometric domain of the channel in Figure 2(a) can be defined as a Boolean (Constructive Solid Geometry) combination of six primitives:

$$\Omega = (f_1 \cup f_2) \cap f_3 \cap f_4 \cap f_5 \cap f_6,$$

where $\overline{x}$ denotes the regularized complement of x, and individual primitives f_1 through f_6 are defined by the following inequalities:

$$f_1 = y \geq 0; \qquad f_2 = x - L_{\text{inlet}} \geq 0; \qquad f_3 = y - s \geq 0;$$
$$f_4 = L_{\text{inlet}} + L_{\text{channel}} - x \geq 0; \qquad f_5 = h_{\text{inlet}} - y \geq 0; \qquad f_6 = x \geq 0$$

Naturally, all numeric constants can be viewed as specific values for some parameters (size, position, etc.). The constructed Boolean representation can be translated into the approximate distance field shown in Figure 2(b) using R-functions:

$$\omega = (f_1 \vee_0 f_2) \wedge_0 f_3 \wedge_0 f_4 \wedge_0 f_5 \wedge_0 f_6, \tag{11}$$

which is also parameterized by h_{inlet}, s, L_{inlet} and L_{channel}. This example clearly shows that any Boolean representation may be translated into the corresponding approximate distance field. Similarly, boundary representation of a solid is a union of solid's faces, each face is a subset of some surface bounded by edges, and so on. This logical description can also be directly translated into a function such that is zero for every point on the boundary and positive elsewhere. Our recent results[35, 41] indicate that such functions can be constructed directly from the commercially available solid modeling representations, as well as from a variety of other geometric data structures, such as cell complexes. For example, Figures 3(a) and (b) show approximate distance fields for the portions of the boundary where non-slip boundary conditions are prescribed (compare to the car shapes in Figures 23(b) and (c) respectively). In the next Section we explain the usage of approximate distance fields for construction of the RFM solution structures and transfinite interpolation of the prescribed boundary conditions.

2.3 RFM solution structure for stream function

A solution structure is a function that satisfies exactly all prescribed boundary conditions. In general, any RFM solution structure can be represented as a sum of two functions:

$$\psi = \psi_0 + \psi_1 \tag{12}$$

where ψ_0 satisfies homogeneous boundary conditions and contains necessary degrees of freedom in order to approximate the differential equation of the problem; function ψ_1 interpolates the functions given as boundary conditions (5),

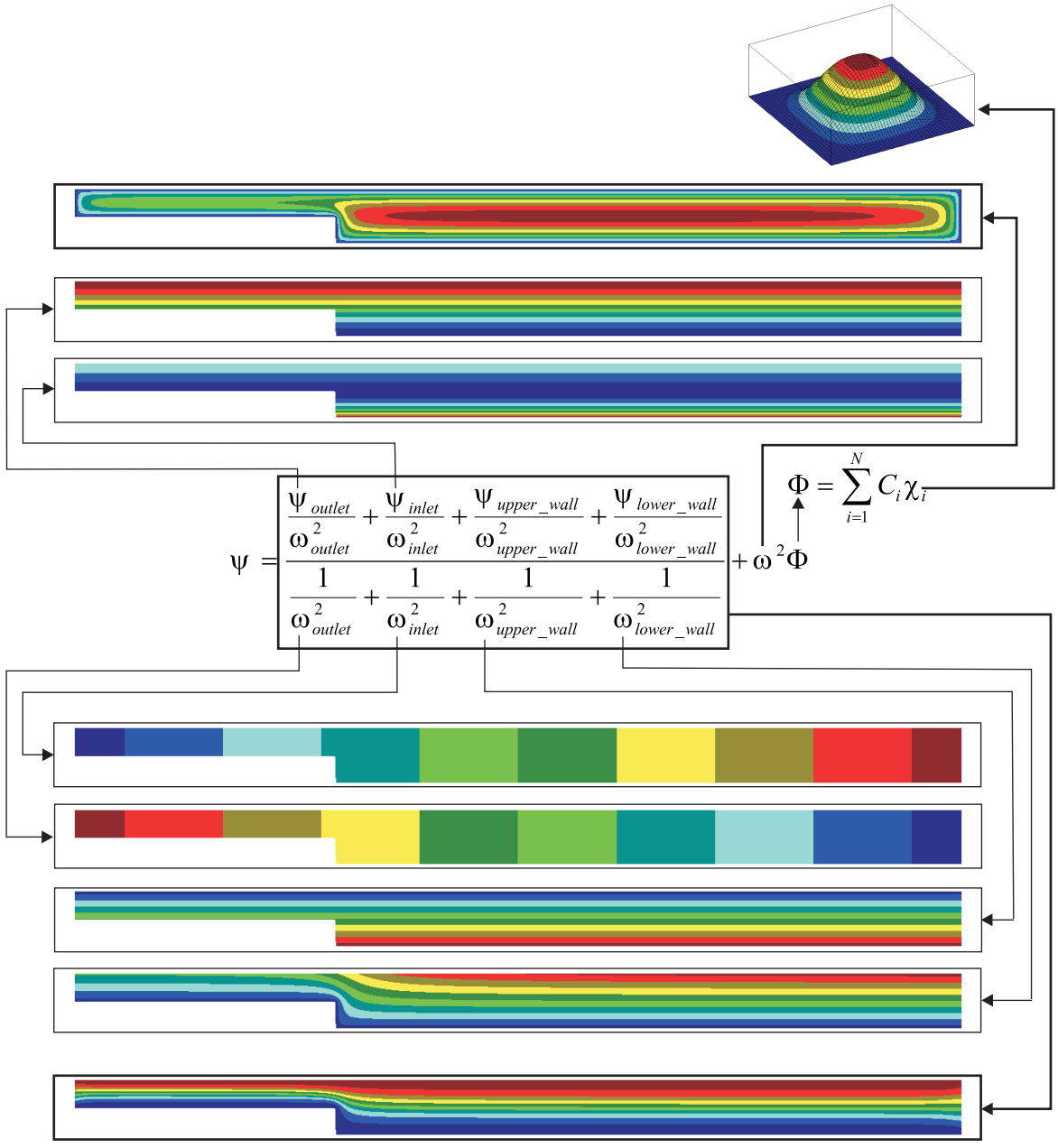

Figure 4: The RFM solution structure that satisfies boundary conditions (4-8) exactly

(6) and (8). The interpolation term is constructed using the transfinite interpolation method [31] which is a generalization of the inverse distance weighting technique; it matches all specified boundary conditions and extends them inside the domain by some arbitrary but well behaved function. For the problem considered here, it takes:

$$\psi_1 = \frac{\frac{\psi_{\text{outlet}}}{\omega^2_{\text{outlet}}} + \frac{\psi_{\text{inlet}}}{\omega^2_{\text{inlet}}} + \frac{\psi_{\text{upper wall}}}{\omega^2_{\text{upper wall}}} + \frac{\psi_{\text{lower wall}}}{\omega^2_{\text{lower wall}}}}{\frac{1}{\omega^2_{\text{outlet}}} + \frac{1}{\omega^2_{\text{inlet}}} + \frac{1}{\omega^2_{\text{upper wall}}} + \frac{1}{\omega^2_{\text{lower wall}}}}, \tag{13}$$

where ω_{outlet}, ω_{inlet}, $\omega_{\text{upper wall}}$ and $\omega_{\text{lower wall}}$ are approximate distance fields that describe outlet, inlet and walls of the channel as it is shown in Figure 4. Rasing these functions to the second power assures that boundary condition $\frac{\partial \psi}{\partial n}_{|\text{whole boundary}} = 0$ is satisfied.

Function ψ_0 in the solution structure (12) serves for approximation of the differential equation of the problem. In our case it can be represented as a product of the second power of an approximate distance to the boundary of the channel ω and unknown function Φ whose sole purpose is the approximation of the differential equation of the problem: $\psi_0 = \omega^2 \Phi$. Since ω takes on zero value on boundary of the geometric domain, ψ_0 vanishes on the boundary together with its first normal derivative. Therefore, regardless of the chosen function Φ, function ψ_0 satisfies the homogeneous boundary conditions exactly. In many practical situations function Φ cannot be determined exactly, which is why it is usually represented by a linear combination of basis functions $\{\chi_i\}_{i=1}^N$:

$$\Phi = \sum_{i=1}^{N} C_i \chi_i. \tag{14}$$

The basis functions $\{\chi_i\}_{i=1}^N$ have to be smooth enough in order to approximate the differential equation of the problem. Thus, the RFM solution structure (12) may be rewritten as follows:

$$\psi = \frac{\frac{\psi_{\text{outlet}}}{\omega^2_{\text{outlet}}} + \frac{\psi_{\text{inlet}}}{\omega^2_{\text{inlet}}} + \frac{\psi_{\text{upper wall}}}{\omega^2_{\text{upper wall}}} + \frac{\psi_{\text{lower wall}}}{\omega^2_{\text{lower wall}}}}{\frac{1}{\omega^2_{\text{outlet}}} + \frac{1}{\omega^2_{\text{inlet}}} + \frac{1}{\omega^2_{\text{upper wall}}} + \frac{1}{\omega^2_{\text{lower wall}}}} + \omega^2 \sum_{i=1}^{N} C_i \chi_i. \tag{15}$$

This solution structure corresponds to the space that contains functions satisfying the prescribed boundary conditions and is sufficiently complete in the sense of being able to approximate the exact solution with an arbitrary degree of accuracy [30].

Employment of the RFM solution structures to represent a solution of a physical problem offers several advantages. In particular: an RFM solution structure treats the prescribed boundary conditions exactly; an RFM solution structure contains no information about the differential equation of the problem which means that the same solution structure can be used to represent solutions of different physical problems with similar types of boundary conditions; basis functions in the solution structure can be constructed over a mesh conforming or non-conforming to a geometric model; solution structure can be easily adjusted to a new geometric model — only approximate distance fields have to be reconstructed in order to represent the boundary pieces of new geometric model; an RFM solution structure can be evaluated and differentiated at *any* point inside the computational domain; finally, an RFM solution structure can be integrated over the geometric model using adaptive numerical procedures [41].

2.4 Computation of the coefficients in the solution structure

Since the RFM solution structure satisfies the given boundary conditions exactly, to solve the problem we need to find the set of the unknown coefficients $\{C_i\}_{i=1}^N$ in the RFM solution structure that gives the best approximation to the differential equation of the boundary value problem. Numerical values of these coefficients can be determined via variational or projectional methods. The differential equation (3) for the stream function contains non-linear terms that have to be linearized before the solution method is applied. After substitution of solution structure (12) into differential

equation (3) and application of Newton-Kantorovich linearization scheme we obtain:

$$\frac{1}{Re}\nabla^4\psi_0^{n+1} - \left(\frac{\partial\psi_0^{n+1}}{\partial y}\frac{\partial\nabla^2\psi_0^n}{\partial x} + \frac{\partial\psi_0^n}{\partial y}\frac{\partial\nabla^2\psi_0^{n+1}}{\partial x} - \frac{\partial\psi_0^{n+1}}{\partial x}\frac{\partial\nabla^2\psi_0^n}{\partial y} - \frac{\partial\psi_0^n}{\partial x}\frac{\partial\nabla^2\psi_0^{n+1}}{\partial y}\right) - \frac{\partial\psi_0^{n+1}}{\partial y}\frac{\partial\nabla^2\psi_1}{\partial x} - \frac{\partial\psi_1}{\partial y}\frac{\partial\nabla^2\psi_0^{n+1}}{\partial x} + \frac{\partial\psi_0^{n+1}}{\partial x}\frac{\partial\nabla^2\psi_1}{\partial y} + \frac{\partial\psi_1}{\partial x}\frac{\partial\nabla^2\psi_0^{n+1}}{\partial y} = -\frac{1}{Re}\nabla^4\psi_1 + \frac{\partial\psi_1}{\partial y}\frac{\partial\nabla^2\psi_1}{\partial x} - \frac{\partial\psi_1}{\partial x}\frac{\partial\nabla^2\psi_1}{\partial y} - \frac{\partial\psi_0^n}{\partial y}\frac{\partial\nabla^2\psi_0^n}{\partial x} + \frac{\partial\psi_0^n}{\partial x}\frac{\partial\nabla^2\psi_0^n}{\partial y}. \tag{16}$$

This equation is formulated for the function ψ_0 satisfying the homogeneous boundary conditions $\psi_0|_{\partial\Omega} = 0$, $\frac{\partial\psi_0}{\partial n}|_{\partial\Omega} = 0$. Equation (16) is solved by an iterative algorithm, and the superscripts $n+1$ and n in the equation denote solutions at the current and previous iterations respectively. The iterative process finishes as soon as the difference between two consecutive solutions becomes sufficiently small. At each iteration the least squares method is applied to equation (16) minimizing the residual of the equation:

$$F = \iint\limits_\Omega \left\{\frac{1}{Re}\nabla^4\psi_0^{n+1} - \left(\frac{\partial\psi_0^{n+1}}{\partial y}\frac{\partial\nabla^2\psi_0^n}{\partial x} + \frac{\partial\psi_0^n}{\partial y}\frac{\partial\nabla^2\psi_0^{n+1}}{\partial x} - \frac{\partial\psi_0^{n+1}}{\partial x}\frac{\partial\nabla^2\psi_0^n}{\partial y} - \frac{\partial\psi_0^n}{\partial x}\frac{\partial\nabla^2\psi_0^{n+1}}{\partial y}\right) - \frac{\partial\psi_0^{n+1}}{\partial y}\frac{\partial\nabla^2\psi_1}{\partial x} - \frac{\partial\psi_1}{\partial y}\frac{\partial\nabla^2\psi_0^{n+1}}{\partial x} + \frac{\partial\psi_0^{n+1}}{\partial x}\frac{\partial\nabla^2\psi_1}{\partial y} + \frac{\partial\psi_1}{\partial x}\frac{\partial\nabla^2\psi_0^{n+1}}{\partial y} + \frac{1}{Re}\nabla^4\psi_1 - \frac{\partial\psi_1}{\partial y}\frac{\partial\nabla^2\psi_1}{\partial x} + \frac{\partial\psi_1}{\partial x}\frac{\partial\nabla^2\psi_1}{\partial y} + \frac{\partial\psi_0^n}{\partial y}\frac{\partial\nabla^2\psi_0^n}{\partial x} - \frac{\partial\psi_0^n}{\partial x}\frac{\partial\nabla^2\psi_0^n}{\partial y}\right\}^2 d\Omega \to min. \tag{17}$$

From the necessary condition of the existence of minimum $\frac{\partial F}{\partial C_i} = 0$, $i = 1, \ldots, N$ we obtain a system of linear equations $\mathbf{AC} = \mathbf{B}$ whose solution gives the numerical values of the unknown coefficients in the solution structure. Elements of the matrix $\mathbf{A}$ and vector $\mathbf{B}$ are defined as follows:

$$a_{ij} = \iint\limits_\Omega \left[\frac{1}{Re}\nabla^4\left(\omega^2\chi_i\right) - \left(\frac{\partial}{\partial y}\left(\omega^2\chi_i\right)\frac{\partial\nabla^2\psi_0^n}{\partial x} + \frac{\partial\psi_0^n}{\partial y}\frac{\partial}{\partial x}\left(\nabla^2\left(\omega^2\chi_i\right)\right) - \frac{\partial}{\partial x}\left(\omega^2\chi_i\right)\frac{\partial\nabla^2\psi_0^n}{\partial y} - \frac{\partial\psi_0^n}{\partial x}\frac{\partial}{\partial y}\left(\nabla^2\left(\omega^2\chi_i\right)\right)\right) - \frac{\partial}{\partial y}\left(\omega^2\chi_i\right)\frac{\partial\nabla^2\psi_1}{\partial x} - \frac{\partial\psi_1}{\partial y}\frac{\partial}{\partial x}\left(\nabla^2\left(\omega^2\chi_i\right)\right) + \frac{\partial}{\partial x}\left(\omega^2\chi_i\right)\frac{\partial\nabla^2\psi_1}{\partial y} + \frac{\partial\psi_1}{\partial x}\frac{\partial}{\partial y}\left(\nabla^2\left(\omega\chi_i\right)\right)\right] \left[\frac{1}{Re}\nabla^4\left(\omega^2\chi_j\right) - \left(\frac{\partial}{\partial y}\left(\omega^2\chi_j\right)\frac{\partial\nabla^2\psi_0^n}{\partial x} + \frac{\partial\psi_0^n}{\partial y}\frac{\partial}{\partial x}\left(\nabla^2\left(\omega^2\chi_j\right)\right) - \frac{\partial}{\partial x}\left(\omega^2\chi_j\right)\frac{\partial\nabla^2\psi_0^n}{\partial y} - \frac{\partial\psi_0^n}{\partial x}\frac{\partial}{\partial y}\left(\nabla^2\left(\omega^2\chi_j\right)\right)\right) - \frac{\partial}{\partial y}\left(\omega^2\chi_j\right)\frac{\partial\nabla^2\psi_1}{\partial x} - \frac{\partial\psi_1}{\partial y}\frac{\partial}{\partial x}\left(\nabla^2\left(\omega^2\chi_j\right)\right) + \frac{\partial}{\partial x}\left(\omega^2\chi_j\right)\frac{\partial\nabla^2\psi_1}{\partial y} + \frac{\partial\psi_1}{\partial x}\frac{\partial}{\partial y}\left(\nabla^2\left(\omega^2\chi_j\right)\right)\right] d\Omega; \tag{18}$$

$$b_i = \iint\limits_\Omega \left[\frac{1}{Re}\nabla^4\left(\omega^2\chi_i\right) - \left(\frac{\partial}{\partial y}\left(\omega^2\chi_i\right)\frac{\partial\nabla^2\psi_0^n}{\partial x} + \frac{\partial\psi_0^n}{\partial y}\frac{\partial}{\partial x}\left(\nabla^2\left(\omega^2\chi_i\right)\right) - \frac{\partial}{\partial x}\left(\omega^2\chi_i\right)\frac{\partial\nabla^2\psi_0^n}{\partial y} - \frac{\partial\psi_0^n}{\partial x}\frac{\partial}{\partial y}\left(\nabla^2\left(\omega^2\chi_i\right)\right)\right) - \frac{\partial}{\partial y}\left(\omega^2\chi_i\right)\frac{\partial\nabla^2\psi_1}{\partial x} - \frac{\partial\psi_1}{\partial y}\frac{\partial}{\partial x}\left(\nabla^2\left(\omega^2\chi_i\right)\right) + \frac{\partial}{\partial x}\left(\omega^2\chi_i\right)\frac{\partial\nabla^2\psi_1}{\partial y} + \frac{\partial\psi_1}{\partial x}\frac{\partial}{\partial y}\left(\nabla^2\left(\omega^2\chi_i\right)\right)\right] \left[-\frac{1}{Re}\nabla^4\psi_1 + \frac{\partial\psi_1}{\partial y}\frac{\partial\nabla^2\psi_1}{\partial x} - \frac{\partial\psi_1}{\partial x}\frac{\partial\nabla^2\psi_1}{\partial y} - \frac{\partial\psi_0^n}{\partial y}\frac{\partial\nabla^2\psi_0^n}{\partial x} + \frac{\partial\psi_0^n}{\partial x}\frac{\partial\nabla^2\psi_0^n}{\partial y}\right] d\Omega \tag{19}$$

Integrals (18) and (19) are computed using adaptive integration algorithm based on the Gauss-Legendre quadrature rule in conjunction with hierarchical space decomposition technique [41].

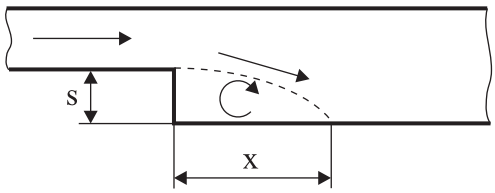

Figure 5: Position of the reattachment point

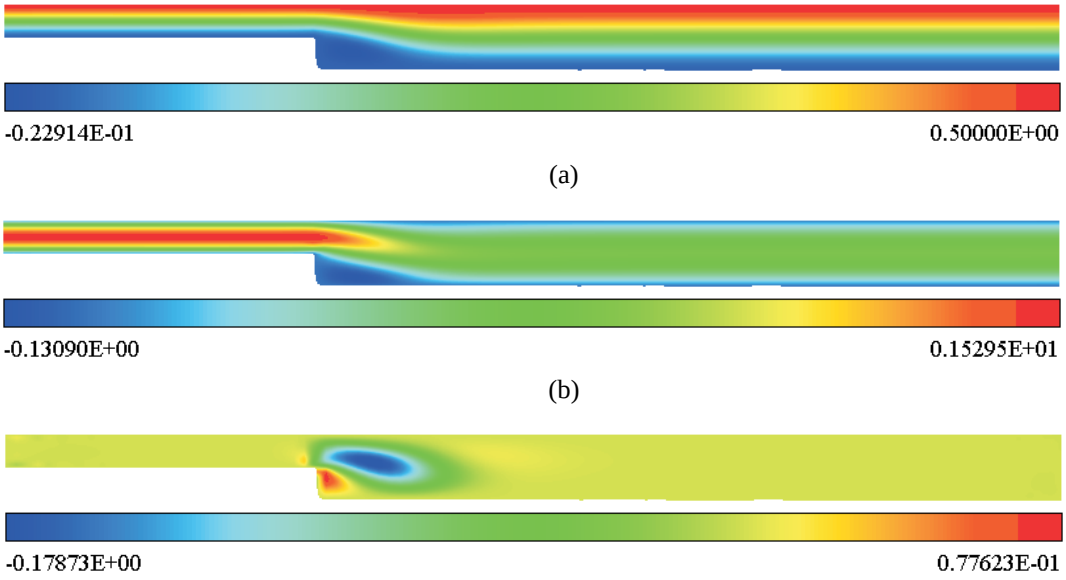

Figure 6: Distributions of (a) stream function, (b) u velocity component and (c) v velocity component for Reynolds number of 100

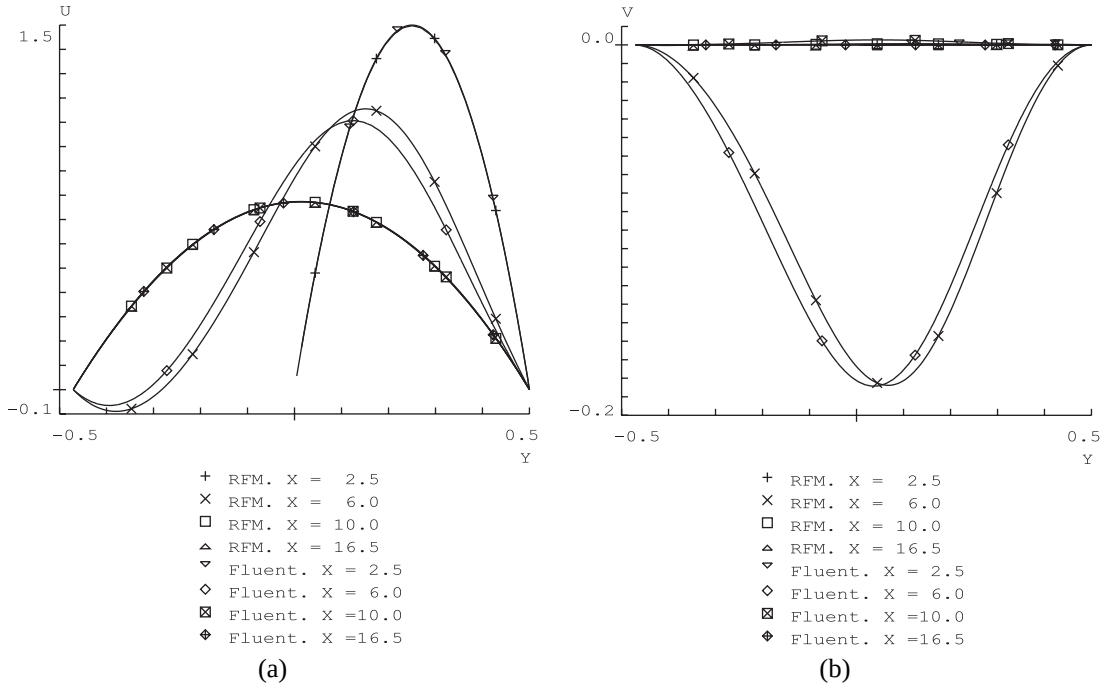

Figure 7: Comparison of the velocity components (a) u and (b) v predicted by RFM and Fluent for $Re = 100$

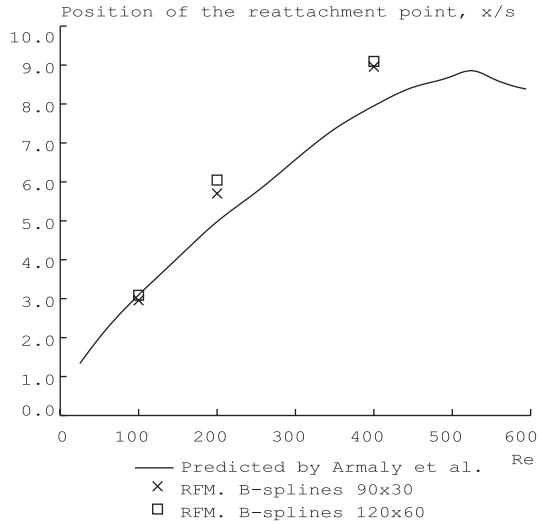

Figure 8: The positions of the reattachment point predicted by RFM using stream function formulation are in good agreement with experimental data given in [2]

Iterations \ Re	1	100	200	400
1	1	1	1	1
2	0.678058E-09	0.329809E-04	0.160996E-03	0.675127E-03
3		0.147665E-06	0.155393E-05	0.376557E-06
4		0.170762E-09	0.889088E-08	0.272996E-06
5				0.534002E-05
6				0.112447E-06
7				0.317925E-07
8				0.408087E-08

Table 1: The relative difference between two consecutive RFM solutions

2.5 Numerical experiments

The above RFM solution procedure was applied to modeling a fluid flow in the back-step channel shown in Figure 1. The stream function ψ is represented by the RFM solution structure (15). The basis functions $\{\chi_i\}_{i=1}^N$ in the solution structure have been chosen as the tensor products of one-dimensional B-splines of the fifth degree, distributed over a uniform rectangular grid. To study the accuracy and convergence properties of the RFM we solve the problem using 90×30 and 120×60 grids of B-splines. The Newton-Kantorovich linearization scheme applied to non-linear equation (3) leads to an iterative solution procedure. The convergence of iterative solutions is achieved when the difference between two consecutive solutions becomes less than prescribed value. In our particular case, we measured the difference between two consecutive solutions by the ratio $\delta = \frac{\sum_{i=1}^{N}(C_i^{n+1}-C_i^n)^2}{\sum_{i=1}^{N}(C_i^{n+1})^2}$. The iterations are stopped as soon as $\delta \leq 10^{-8}$. Table 1 illustrates fast convergence of the RFM solutions for Reynolds numbers 1, 100, 200 and 400 computed over 90×30 uniform rectangular grid of B-splines. The number of iterations, which are necessary to achieve the convergent solution, increases with Reynolds number, but in all cases it does not exceed 10.

Comparison of Figures 6(b) and 6(c) with Figures 14(a) and 14(b), respectively, demonstrates that distributions of the velocity components u and v computed by the RFM for $Re = 100$ over 120×60 grid of B-splines are almost identical with the velocity components predicted by the commercial fluid dynamics system Fluent. Figures 7(a) and 7(b), presenting plots of velocity components u and v in several cross sections of the channel, illustrate good agreement of the results computed by the RFM and Fluent. In addition, for Reynolds numbers 100, 200 and 400, we computed the position of the reattachment point (see Figure 5). Figure 8 illustrates good agreement of the position of the reattachment point predicted by RFM for $Re = 100$ with experimental data given in [2]. For Reynolds numbers 200 and 400, the RFM solution overestimated the position of the reattachment point by about 10%. Figure 8 also shows little changes in the results given by RFM for 90×30 and 120×60 grids of B-splines which further indicates convergence of the approximate solution of the problem.

The stream function formulation is rarely used to solve incompressible fluid dynamics problems because it experiences difficulties with assigning boundary conditions to the walls of multiply-connected channels. Moreover this formulation of fluid dynamics problem does not generalize easily for three dimensional flows. Therefore, in many practical situations Navier-Stokes and continuity equations are solved directly. In the next Section we show that such direct solutions may be also obtained by the meshfree RFM.

3 Direct solution of the Navier-Stokes problem

In this Section we discuss application of the RFM to direct solution of Navier-Stokes problem using an artificial compressibility approach. First, we explain the elements of the RFM solution structures for the velocity components

and pressure. Then we describe an iterative solution algorithm that treats the modified Navier-Stokes and the pressure equations. The Section finishes with analysis of the RFM modeling results and their comparison with experimental data and numerical solutions given by the commercial system Fluent.

3.1 An artificial compressibility approach

With the well known artificial compressibility approach [39], the solution for an incompressible fluid is obtained in this case as a limit of the solution for non-steady Navier-Stokes problem as the artificial time approaches a sufficiently high value. In this case, solution of the incompressible fluid dynamics problem leads to the integration of the following system of partial differential equations [39]:

$$\begin{aligned}
&\frac{\partial u}{\partial t} + u\frac{\partial u}{\partial x} + v\frac{\partial u}{\partial y} - \frac{1}{Re}\nabla^2 u = -Eu\frac{\partial p}{\partial x};\\
&\frac{\partial v}{\partial t} + u\frac{\partial v}{\partial x} + v\frac{\partial v}{\partial y} - \frac{1}{Re}\nabla^2 v = -Eu\frac{\partial p}{\partial y};\\
&\frac{\partial p}{\partial t} = -a^2\left(\frac{\partial u}{\partial x} + \frac{\partial v}{\partial y}\right),
\end{aligned} \tag{20}$$

where a is an artificial sound speed, and t is an artificial time. The system of equations (20) describes the pressure and velocity distributions away from the boundary of the computational domain. However, the velocity and pressure fields depend very much on the geometry of the channel. This dependence is described by the boundary conditions, which are formulated as a known velocity profile at the inlet, zero velocity values at the walls, and zero normal derivative of the velocity at the outlet:

$$\begin{aligned}
&u_{|\text{inlet}} = \varphi_u(x,y) = 6\left(\frac{y}{h_{\text{inlet}}} - \frac{y^2}{h_{\text{inlet}}^2}\right);\\
&v_{|\text{inlet}} = \varphi_v(x,y) = 0;\\
&u_{|\text{walls}} = 0;\\
&v_{|\text{walls}} = 0;\\
&\frac{\partial u}{\partial n}_{|\text{outlet}} = 0;\\
&\frac{\partial v}{\partial n}_{|\text{outlet}} = 0;
\end{aligned} \tag{21}$$

where φ_u and φ_v describe the velocity profile at inlet and n is the outward normal of the computational domain.

3.2 Vector RFM solution structures

The vector of unknowns for the considered Navier-Stokes problem consists of three components: two components of the velocity vector and pressure. A solution structure has to be constructed for each of the three unknown functions. Because the types of boundary conditions for the velocity components u and v are the same, we explicitly show the solution structure for the u component only. The solution structure for v is obtained by syntactic replacement of symbols "u" by symbols "v". According to [28], the solution structure satisfying boundary conditions (21) for velocity components may be written as sum of homogeneous and non-homogeneous terms:

$$u = u_0 + u_1, \tag{22}$$

where function

$$u_1 = -\frac{\omega_{\text{inlet+walls}}\omega_{\text{outlet}}}{\omega_{\text{inlet+walls}} + \omega_{\text{outlet}}} D_1^{\omega_{\text{outlet}}}\left(\varphi_u^*\right) + \varphi_u^*, \tag{23}$$

satisfies non-homogeneous boundary conditions; and function

$$u_0 = \omega_{\text{inlet+walls}}\Phi_u - \frac{\omega_{\text{inlet+walls}}\omega_{\text{outlet}}}{\omega_{\text{inlet+walls}} + \omega_{\text{outlet}}} D_1^{\omega_{\text{outlet}}}\left(\omega_{\text{inlet+walls}}\Phi_u\right) = \sum_{i=1}^{N_u} C_i^u u_{0i}, \tag{24}$$

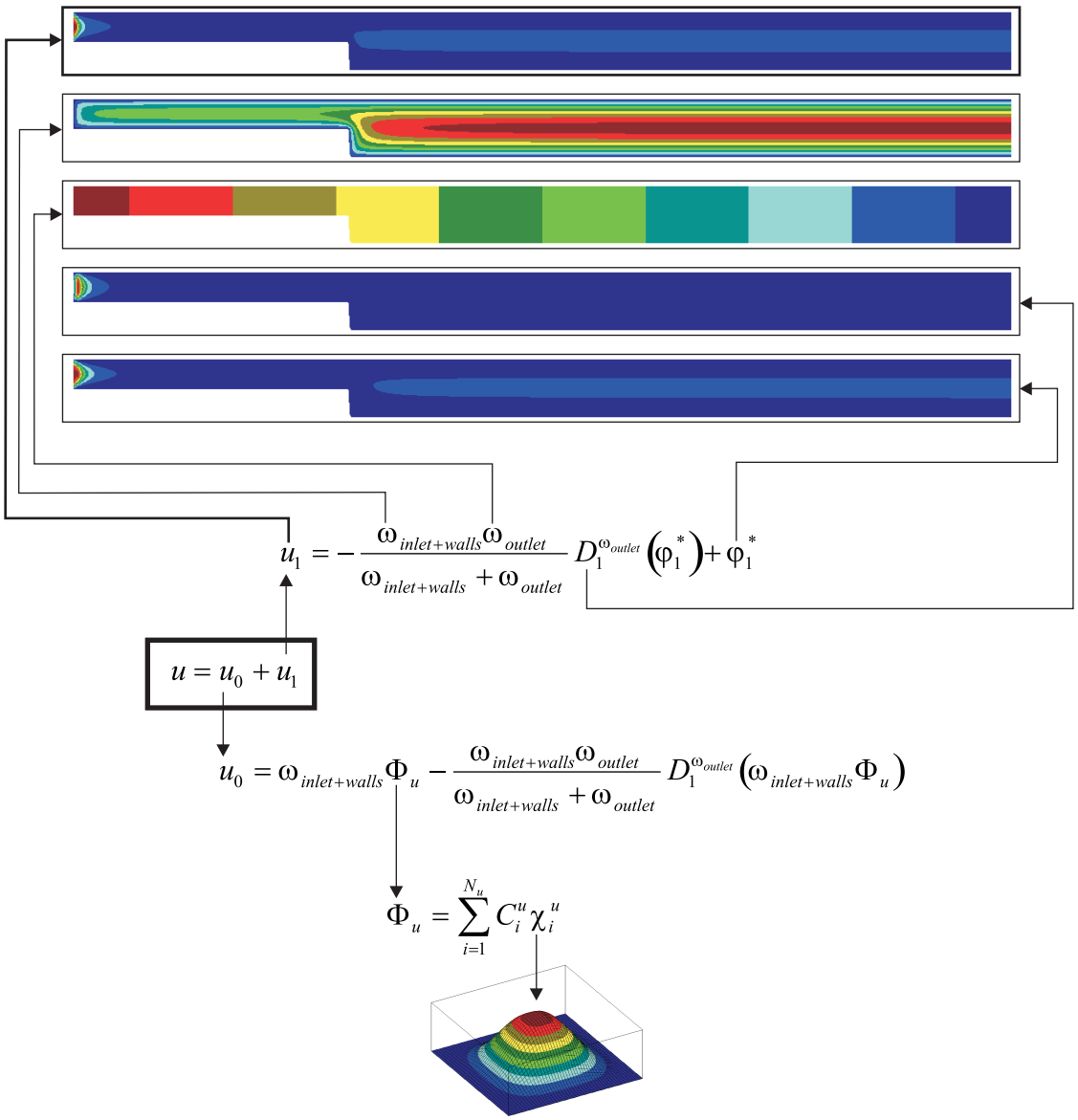

Figure 9: An RFM solution structure that satisfies boundary conditions (21) exactly

is a linear combinations of the basis functions satisfying homogeneous boundary conditions exactly. Function $\varphi_u^* = \frac{\varphi_u \omega_{\text{walls}}}{\omega_{\text{walls}} + \omega_{\text{inlet}}}$ transfinitely interpolates the given velocity values at the inlet and at the walls of the channel; zero sets of the approximate distance functions ω_{outlet}, ω_{inlet} and ω_{walls} describe the geometry of the outlet, inlet and walls, respectively as shown in Figure 9. Similarly to the solution structure for the stream function, the unknown function Φ_u is represented as linear combinations of basis functions:

$$\Phi_u = \sum_{i=1}^{N_u} C_i^u \chi_i^u.$$

The operator $D_1^\omega() = \nabla\omega\nabla()$ is a differential operator in the normal direction to the boundary.

Since no boundary conditions are set for the pressure field, its distribution may be represented by the unknown function Φ_p:

$$p = \Phi_p = \sum_{i=1}^{N} C_i^p \chi_i^p. \tag{25}$$

3.3 Application of the least squares method

Here we describe the solution procedure for the incompressible fluid dynamics problem using the artificial compressibility approach. The solution structure contains no information about the differential equation of the problem; rather it defines a functional space satisfying the given boundary conditions. The function approximating the solution of the boundary value problem may be chosen from this space via some numerical procedure for computing the values of the unknown coefficients in the solution structure. The equations (20) are non-linear and describe the non-steady physical process. To solve this system of equations we discretize them by artificial time and, after linearization, we obtain:

$$\begin{aligned}
&\frac{u_{n+1}}{\triangle t} + u_n \frac{\partial u_{n+1}}{\partial x} + v_n \frac{\partial u_{n+1}}{\partial y} - \frac{1}{Re}\nabla^2 u_{n+1} = -Eu\frac{\partial p_{n+1}}{\partial x} + \frac{u_n}{\triangle t};\\
&\frac{v_{n+1}}{\triangle t} + u_n \frac{\partial v_{n+1}}{\partial x} + v_n \frac{\partial v_{n+1}}{\partial y} - \frac{1}{Re}\nabla^2 v_{n+1} = -Eu\frac{\partial p_{n+1}}{\partial y} + \frac{v_n}{\triangle t};\\
&p_{n+1} = p_n - a^2 \triangle t \left(\frac{\partial u_n}{\partial x} + \frac{\partial v_n}{\partial y}\right).
\end{aligned} \tag{26}$$

Here u_{n+1}, v_{n+1} and p_{n+1} are the velocity components and pressure at the current time instance; u_n, v_n and p_n are the velocity components and pressure at the previous time instance (for the stream function formulation the iteration number is the superscript, here subscript is used); $\triangle t$ is the time step.

To solve for the coefficients $C^{u,v,p}$ in solution structures (22) and (25) we apply the least squares method to the discretized equation (26). Substituting solution structures (25) and (22) into differential equations (26) and applying the least squares method, we obtain systems of linear algebraic equations whose solutions give numerical values of the coefficients C^u, C^v, and C^p:

- from the X momentum equation: $\mathbf{A}^u \mathbf{C}^u = \mathbf{B}^u$, where

$$\begin{aligned}
a_{ij}^u &= \iint\limits_\Omega \left(\frac{u_{0i}}{\triangle t} + u_n \frac{\partial u_{0i}}{\partial x} + v_n \frac{\partial u_{0i}}{\partial y} - \frac{1}{Re}\nabla^2 u_{0i}\right)\left(\frac{u_{0j}}{\triangle t} + u_n \frac{\partial u_{0j}}{\partial x} + v_n \frac{\partial u_{0j}}{\partial y} - \frac{1}{Re}\nabla^2 u_{0j}\right) d\Omega\\
b_i^u &= \iint\limits_\Omega \left(\frac{u_{0i}}{\triangle t} + u_n \frac{\partial u_{0i}}{\partial x} + v_n \frac{\partial u_{0i}}{\partial y} - \frac{1}{Re}\nabla^2 u_{0i}\right)\\
&\quad \left(-Eu\frac{\partial p_{n+1}}{\partial x} + \frac{u_n - u_1}{\triangle t} - u_n \frac{\partial u_1}{\partial x} - v_n \frac{\partial u_1}{\partial y} + \frac{1}{Re}\nabla^2 u_1\right) d\Omega
\end{aligned}$$

- from the Y momentum equation: $\mathbf{A}^v\mathbf{C}^v = \mathbf{B}^v$, where

$$a_{ij}^v = \iint\limits_{\Omega} \left(\frac{v_{0i}}{\triangle t} + u_n\frac{\partial v_{0i}}{\partial x} + v_n\frac{\partial v_{0i}}{\partial y} - \frac{1}{Re}\nabla^2 v_{0i}\right)\left(\frac{v_{0j}}{\triangle t} + u_n\frac{\partial v_{0j}}{\partial x} + v_n\frac{\partial v_{0j}}{\partial y} - \frac{1}{Re}\nabla^2 v_{0j}\right) d\Omega$$

$$b_i^v = \iint\limits_{\Omega} \left(\frac{v_{0i}}{\triangle t} + u_n\frac{\partial v_{0i}}{\partial x} + v_n\frac{\partial v_{0i}}{\partial y} - \frac{1}{Re}\nabla^2 v_{0i}\right) \left(-Eu\frac{\partial p_{n+1}}{\partial y} + \frac{v_n - v_1}{\triangle t} - u_n\frac{\partial v_1}{\partial x} - v_n\frac{\partial v_1}{\partial y} + \frac{1}{Re}\nabla^2 v_1\right) d\Omega$$

- from the pressure equation: $\mathbf{A}^p\mathbf{C}^p = \mathbf{B}^p$, where

$$a_{ij}^p = \iint\limits_{\Omega} \chi_i^p \chi_j^p d\Omega$$

$$b_i^p = \iint\limits_{\Omega} \chi_i^p \left(p_n - a^2\left(\frac{\partial u_n}{\partial x} + \frac{\partial v_n}{\partial y}\right)\right) d\Omega$$

These three systems of linear equations are solved sequentially starting with the pressure equation. As soon as the new pressure distribution is computed it is used to solve the momentum equations. At every iteration we check the approximation error of the momentum and continuity equations by computing the following residuals:

$$\begin{aligned} R_u &= \frac{1}{A}\sqrt{\iint\limits_{\Omega}\left(u\frac{\partial u}{\partial x} + v\frac{\partial u}{\partial y} - \frac{1}{Re}\nabla^2 u + Eu\frac{\partial p}{\partial x}\right)^2 d\Omega}; \\ R_v &= \frac{1}{A}\sqrt{\iint\limits_{\Omega}\left(u\frac{\partial v}{\partial x} + v\frac{\partial v}{\partial y} - \frac{1}{Re}\nabla^2 v + Eu\frac{\partial p}{\partial y}\right)^2 d\Omega}; \\ R_p &= \frac{1}{A}\sqrt{\iint\limits_{\Omega}\left(\frac{\partial u}{\partial x} + \frac{\partial v}{\partial y}\right)^2 d\Omega}, \end{aligned} \tag{27}$$

where A is the area of the computational domain. As soon as the residuals R_u, R_v and R_p become smaller than a prescribed value the iterative process is finished.

Since the artificial compressibility approach leads to non-steady equations (20), it is necessary to add the initial conditions to the problem statement. Sometimes it is convenient to choose as the initial distributions for the velocity components functions u_1 and v_1 given by expression (23):

$$\begin{aligned} u_{|t=0} &= u_1; \\ v_{|t=0} &= v_1; \end{aligned} \tag{28}$$

and uniform pressure within the computational domain:

$$p_{|t=0} = 0. \tag{29}$$

3.4 Numerical properties of the RFM solutions

This numerical experiment illustrates the accuracy and convergence of the RFM applied to direct solution of Navier-Stokes problem via artificial compressibility approach. Computations were performed for four Reynolds numbers: 1, 100, 200 and 400. Components u and v of the velocity vector and the pressure p are represented by RFM solution structures (22) and (25). Basis functions $\{\chi_i^u\}_{i=1}^{N_u}$ and $\{\chi_i^v\}_{i=1}^{N_v}$ have been chosen to be bicubic B-splines defined on a uniform 120×60 rectangular grid. The order of the basis functions $\{\chi_i^p\}_{i=1}^{N_p}$, approximating the pressure field, can be

lowered, since the pressure equation (26) contains no derivatives of p with respect to spatial variables. Therefore we choose the basis functions $\{\chi_i^p\}_{i=1}^{N_p}$ to be bilinear B-splines defined on a uniform 120×60 rectangular grid.

Distributions of the velocity components and pressure predicted by the RFM are given in Figures 10, 11, 12 and Figure 13 for Reynolds numbers 1, 200, 400 and 100 respectively. Accuracy of the computations is confirmed by comparison of the solutions obtained by RFM with solutions produced by the commercial fluid dynamics solver Fluent. For example, comparison of Figure 13 and Figure 14 shows that the velocity distributions and the pressure fields computed by the RFM and Fluent exhibit almost no difference. Figure 15 illustrates good agreement of the velocity components predicted by RFM and Fluent in several cross sections of the channel for the case of $Re = 100$. The plot given in Figure 16 demonstrates that the positions of the reattachment point computed via RFM for different Reynolds numbers coincide with the experimental data from [2]. As the Reynolds number increases, more time steps (iterations) are needed to achieve the convergent solution.

The convergence of the iterative RFM solutions was observed using the following criteria:

- Discharge $q = \int\limits_{y_{min}}^{y_{max}} u(x,y)dy$ through the specified sections of the channel. This is a physical criterion of convergence, which estimates the quality of approximation of the continuity equation. Figure 17 proves convergence of solutions given by the RFM showing that the total discharge through different cross sections of the channel approaches the same nominal value. The convergence rate is rapid at the initial stages of the computation, but slows down substantially after approaching about 80% of the expected value.

- Relative error in the computed coefficients. This is given by ratios $\delta^{u,v,p} = \frac{||C_{n+1}^{u,v,p} - C_n^{u,v,p}||}{||C_{n+1}^{u,v,p}||}$, where $C_{n+1}^{u,v,p}$ and $C_n^{u,v,p}$ are the vectors of coefficients at the nth and $(n+1)$th iterations. Since the same solution structures represent solutions at the current and previous iterations, these solutions differ from each other by the coefficients only. Therefore values of $\delta^{u,v,p}$ estimate th difference between two consecutive solutions. The plots given in Figures 18(a) and (b) indicate unanimously that the iterative RFM solutions satisfy the necessary condition of convergence — the difference between two consecutive solutions decreases rapidly with the number of iterations.

- Averaged residuals computed by formulas (27) estimate the values of least squares functionals which are minimized on each iteration. At the beginning of computations averaged residuals rapidly change their values, but after completing approximately 10% of the iterations needed to reach the convergent solution, the values of the averaged residuals stabilize (see Figure 19).

We have observed that the type and properties of the approximate distance fields may have a substantial effect on convergence. For example, when distance fields are constructed using boundary representations approximately 1.5 times more iterations are required than for approximations constructed directly from Constructive Solid Geometry models. This phenomenon is explained by the different smoothness properties of the distance fields in the neighborhoods of the sharp corners [35]. However, in all cases, the solutions obtained by RFM are reasonable both in accuracy and convergence. The plots of the pressure and the v component of the velocity vector appear to have oscillatory behavior in the cross section just after the back-step (Figure 20). But such oscillations are common with employment of the Galerkin method [6, 12] for incompressible fluid flow problems. Indeed, in our case, the application of the least squares method to the pressure equation is identical to the Galerkin method, which explains the observed fluctuations and even occasional increases in average residuals.

A crucial test for a meshfree method such as RFM is independence of the solution from the particular alignment or orientation of the mesh. But for application of the RFM this non-alignment is often expected. Figure 21 shows the backward facing step channel rotated 5 degrees relative to the background mesh. Figure 22 presents distributions of u and v components of the velocity vector, its absolute value $|\mathbf{V}| = \sqrt{u^2 + v^2}$ and pressure p predicted by the RFM. The results illustrate independence of the RFM solution from the orientation of the geometric model with respect to the underlying grid of B-splines. In fact, the distributions of the absolute value of the velocity vector inside the rotated channel (Figure 22(c)) and inside the channel shown in Figure 1 are identical.

4 Conclusions

We stress that all constructions described in this paper are completely general and fully automatic. The symbolic manipulations shown here are mainly for the benefit of the readers, and the restriction to the backstep geometry is used only to facilitate careful numerical studies. As implemented, the method is fully automatic and applies to any two-dimensional geometry. For example, fluid flow models for various car shapes inside a wind tunnel are shown in Figures 23(a), (b) and (c). Figures 24, 25 and 26 present the distributions of the pressure field and the u velocity component for each car shape respectively. These computations were performed for a Reynolds number of 100. In all cases, the distance fields and solution structures are assembled automatically from the user specified geometry and boundary conditions using techniques described in [35, 31, 41]. The constructed functions are also automatically differentiated and integrated as required for the numerical solution of the problem using computational methods of [36, 41, 40]. Subsequent changes in geometry require no manual tasks, meshing, or other type of spatial discretizations. Thus, it should be clear that the method holds great promise for automatic solution of computational fluid dynamics problems and subsequent shape and design optimization tasks.

The meshfree RFM is based on the ability to satisfy any and all types of boundary conditions without a conforming mesh. As such, it is not critically dependent on the use of the Galerkin method, and can be combined with other numerical methods. The present studies indicate that convergence properties of the RFM are certainly acceptable, but are substantially affected by the associated numerical procedures. Further efforts on improving numerical properties of the method should be focused on combining RFM with other types of numerical procedures that are known to exhibit good numerical properties. For example, it is known that the artificial compressibility approach (used in our experiments) often requires large numbers of iterations and may lead to less accurate solutions. Instead, RFM could be combined with a much faster, though less stable, pressure correction approach. A number of methods have been developed in order to increase stability of the pressure correction approach [39], but all these numerical schemes are oriented towards finite difference methods. Similarly, in order to eliminate the oscillatory behavior, one should not use the variational methods for determining the unknown coefficients in the RFM solution structure. Rather, one should rely on other established procedures, such as finite differences. Thus, combining RFM with finite differences appears to be one of the more promising directions that may result in a method combining the flexibility and mesh-freedom of RFM with the attractive numerical properties of the proven finite difference techniques. Accuracy, stability and the rate of convergence of the RFM solutions can be substantially improved using regularized Navier-Stokes equations [10]. The regularization approach proved its good numerical properties for two and three-dimensional problems as well as for the wide range of the Reynolds numbers.

Acknowledgments

This work was supported in part by the National Science Foundation grants DMI-9900171, DMI-9522806, CCR-9813507, the NATO Linkage grant PST.CLG.976192, General Motors Corporation, and Intact Solutions, LLC. The authors are grateful to V.L. Rvachev, T.I. Sheyko, C. Rutland for providing a number of useful suggestions; to A. Duarte and A. Fedoseyev for reading the draft of the paper and for their critical comments. The authors also express their gratitude to Dr. Sumantran for his support and guidance during the initial stage of the project.

References

[1] M. Aftosmis, J. Melton, and Berger M. Robust and efficient Cartesian mesh generation for component-based geometry. *AIAA J.*, 36(6), 1998.

[2] B. F. Armaly, F. Durst, J. C. F. Pereira, and B. Schonung. Experimental and theoretical investigation of backward-facing step flow. *J. Fluid Mech.*, 127:473–496, 1983.

[3] T. Belytschko, Y. Krongauz, D. Organ, M. Fleming, and P. Krysl. Meshless methods: An overview and recent developments. *Computer Methods in Applied Mechanics and Engineering*, 139(1–2):3–47, 1996.

[4] T. Belytschko, Y. Y. Lu, and L. Gu. Element-free Galerkin methods. *Int. J. Numeric. Methods Engrg.*, 37:229–256, 1994.

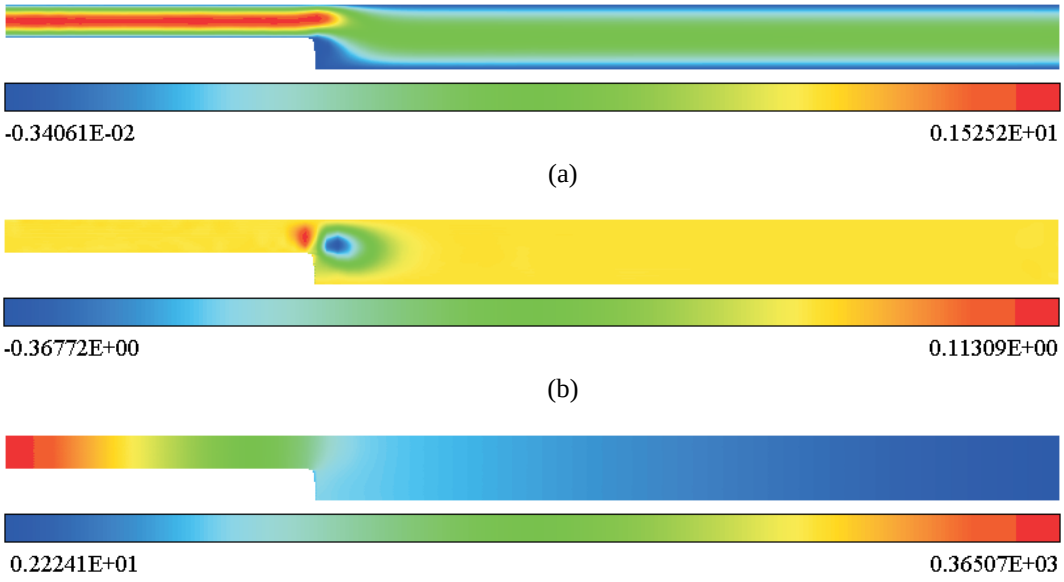

Figure 10: Distributions of (a) u velocity component, (b) v velocity component and (c) pressure obtained by direct solution of Navier-Stokes problem for Reynolds number of 1 given by RFM

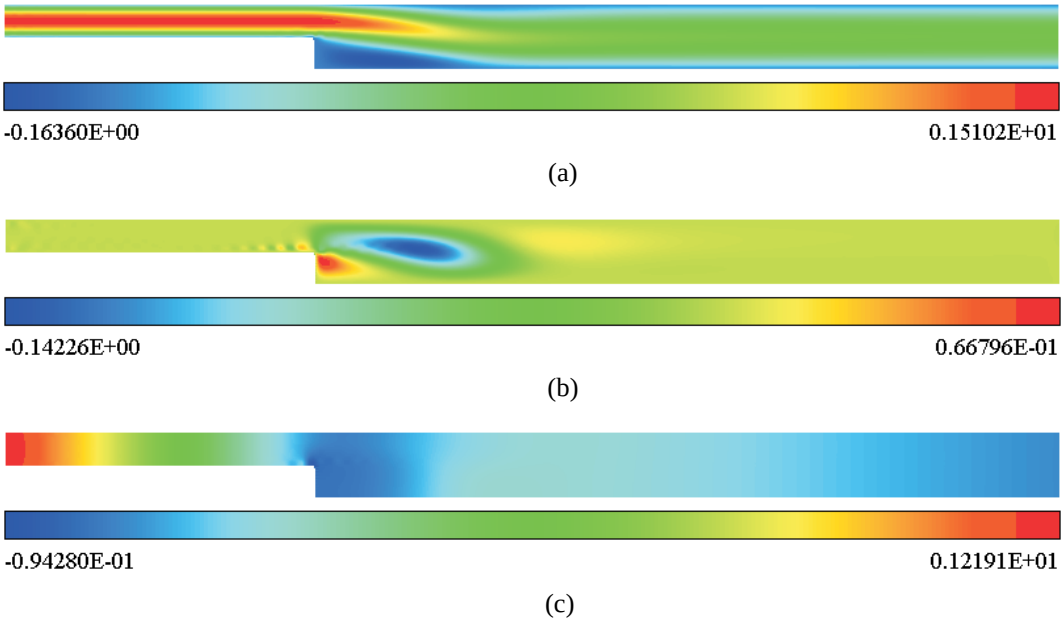

Figure 11: Distributions of (a) u velocity component, (b) v velocity component and (c) pressure obtained by direct solution of Navier-Stokes problem for Reynolds number of 200 given by RFM

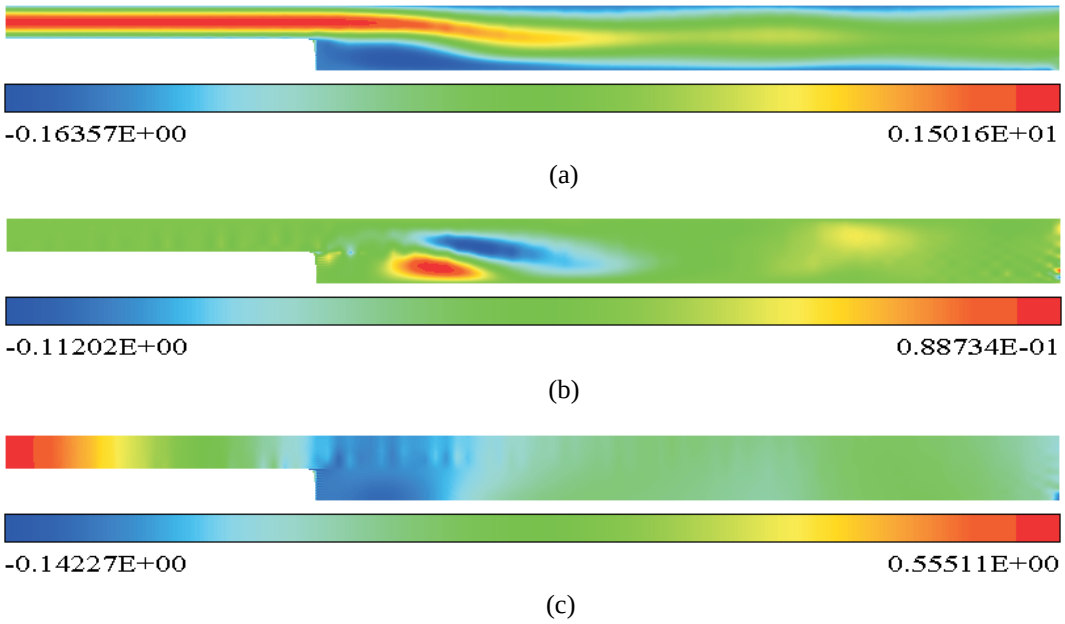

Figure 12: Distributions of (a) u velocity component, (b) v velocity component and (c) pressure obtained by direct solution of Navier-Stokes problem for Reynolds number of 400 given by RFM

[5] M. Berger and M. Aftosmis. Parallel multigrid on Cartesian meshes with complex geometry. In *Proceedings of the 8th Intl. Conference on Parallel CFD*, Trondheim, Norway, May, 2000.

[6] A. N. Brooks and T. J. R. Hughes. Streamline upwind/petrov-galerkin formulation for convection dominated flows with particular emphasis on incompressible navier-stokes equations. *Computer Methods in Applied Mechanics and Engineering*, 32:199–259, 1982.

[7] J.-S. Chen, C. Pan, C.M.O.L. Roque, and H.-P. Wang. A lagrangian reproducing kernel particle method for metal forming analysis. *Computational Mechanics*, 22:289–307, 1998.

[8] J.-S. Chen and H.-P. Wang. New boundary condition treatments for meshless computation of contact problems. *Computer Methods in Applied Mechanics and Engineering*, 1999. in press.

[9] C. A. Duarte and J. T. Oden. An h-p adaptive methods using clouds. *Computer Methods in Applied Mechanics and Engineering*, 139:237–262, 1996.

[10] A.I. Fedoseyev. A regularization approach to solving the navier-stokes equations for problems with boundary layers. *Computational Fluid Dynamics J.*, pages 317–324, 2001. Special Issue.

[11] H. Forrer and M. Berger. Flow simulations on Cartesian grid involving complex moving geometries. In *Proceedings of the 7th International Conference on Hyperbolic Problems*, Zurich, Switzerland, February, 1998.

[12] L. P. Franca and A. Nesliturk. On a two level finite element method for incompressible navier-stokes equations. *Int. J. Numer. Meth. Engng*, 52:433–453, 2001.

[13] Frank C. Gunter and Wing Kam Liu. Implementation of boundary conditions for meshless methods. *Computer Methods in Applied Mechanics and Engineering*, 163:205–230, 1998.

[14] Mohd-Yusof J. Combined immersed boundary/B-spline methods for simulations of flow in complex geometries. Ctr annual research briefs, NASA Ames Research Center/Stanford Univ. Center for Turbulence Research, Stanford, CA, 1997.

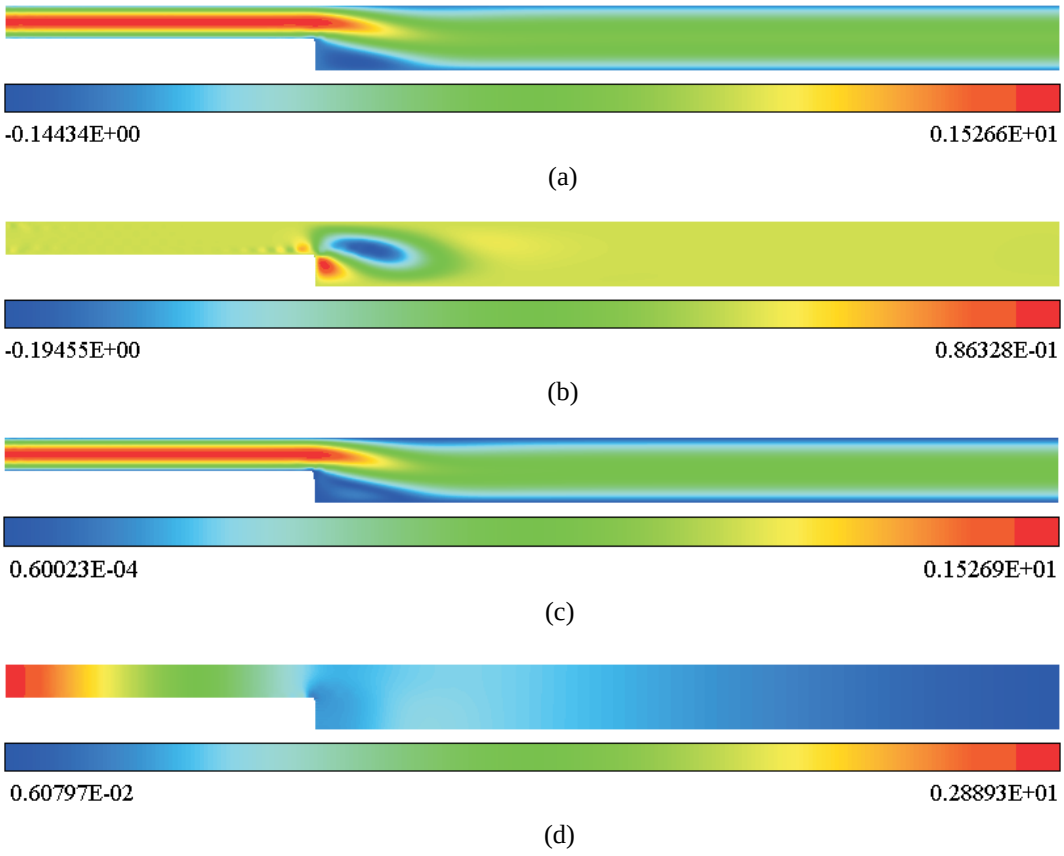

Figure 13: Distributions of (a) u velocity component, (b) v velocity component, (c) absolute value of the velocity vector $|\mathbf{V}| = \sqrt{u^2 + v^2}$ and (d) pressure obtained by direct solution of Navier-Stokes problem for Reynolds number of 100 given by RFM

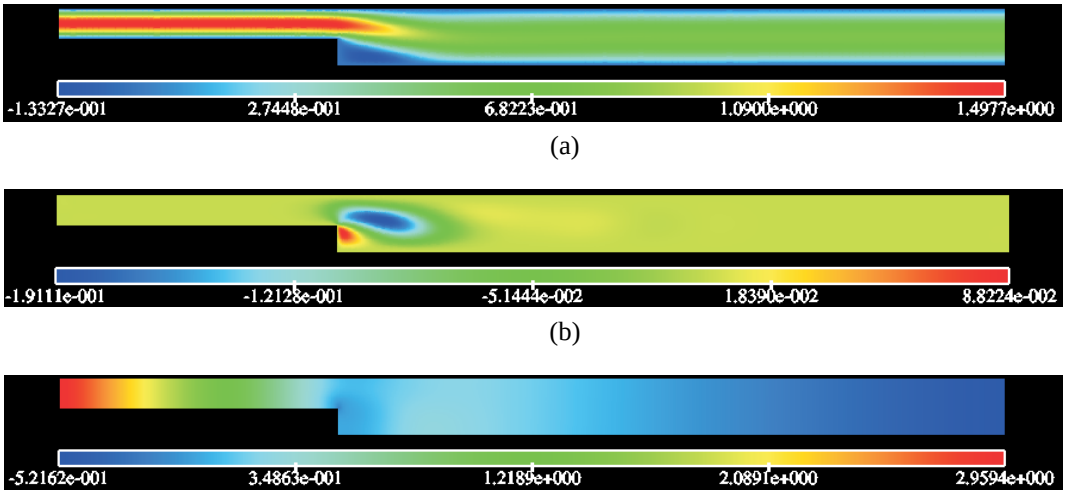

Figure 14: Distributions of (a) u velocity component, (b) v velocity component and (c) pressure obtained by direct solution of Navier-Stokes problem for Reynolds number of 100 given by commercial system Fluent

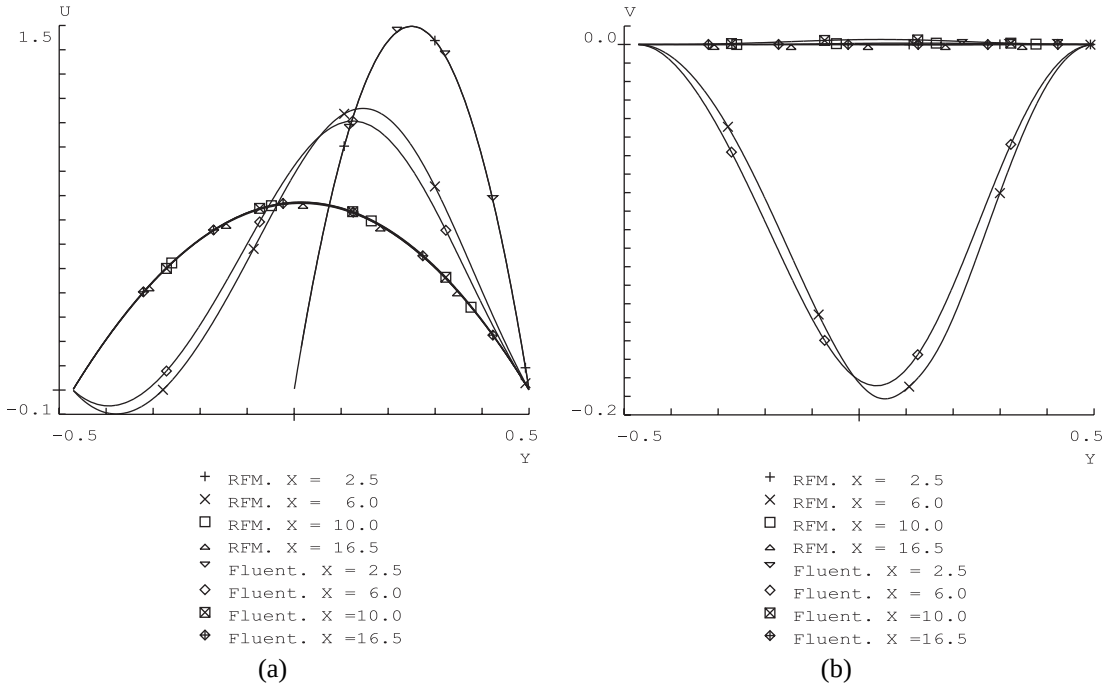

Figure 15: Comparison of the velocity components (a) u and (b) v predicted by RFM and Fluent for $Re = 100$

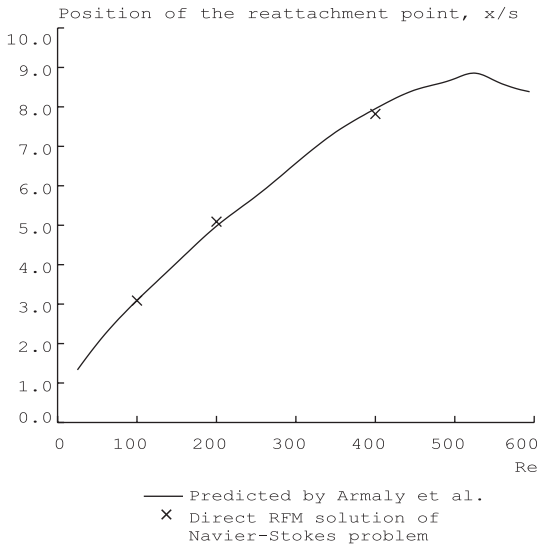

Figure 16: The positions of the reattachment point predicted by RFM using an artificial compressibility approach coincide with experimental data given in [2]

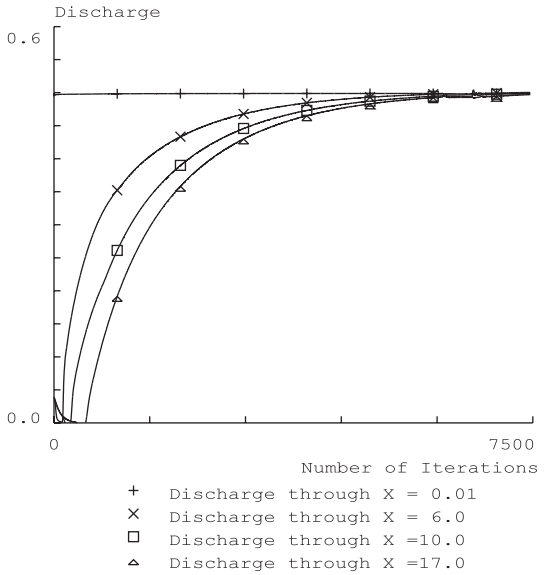

Figure 17: Discharge through cross sections of the channel converges to the same value ($Re = 100$)

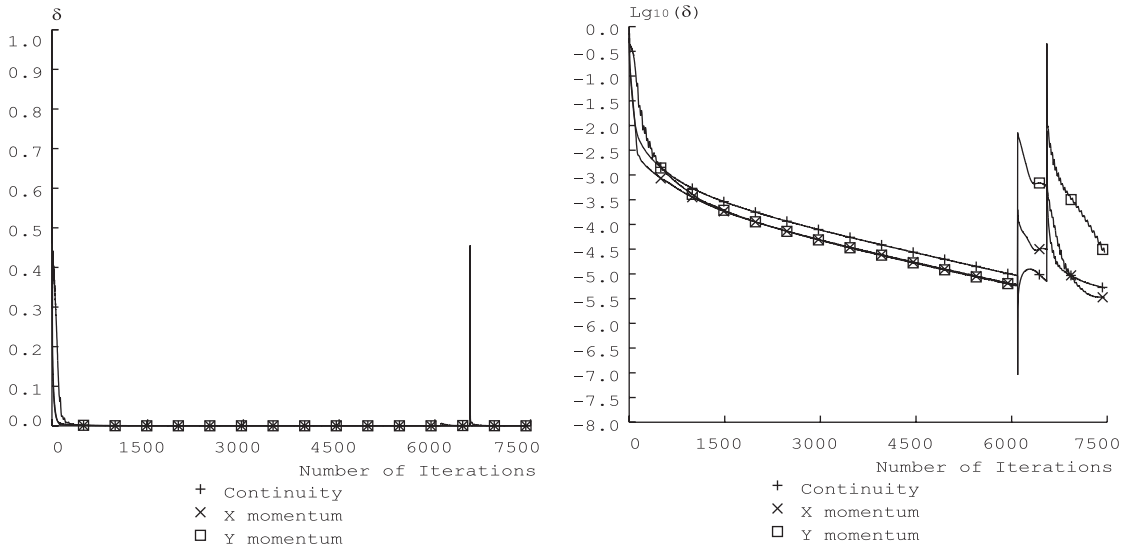

Figure 18: (a) Relative distances $\delta^{u,v,p} = \frac{||C_{n+1}^{u,v,p} - C_n^{u,v,p}||}{||C_{n+1}^{u,v,p}||}$ between two consecutive RFM solutions and (b) their logarithms $lg_{10}(\delta^{u,v,p})$ decrease with number of iterations ($Re = 100$)

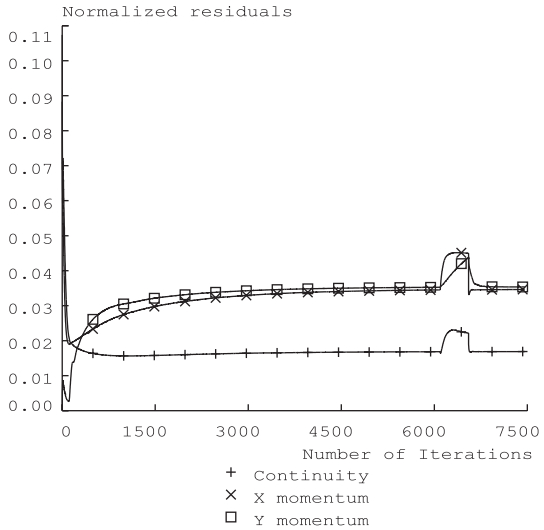

Figure 19: Dependence of the normalized residuals (27) on the number of iterations ($Re = 100$)

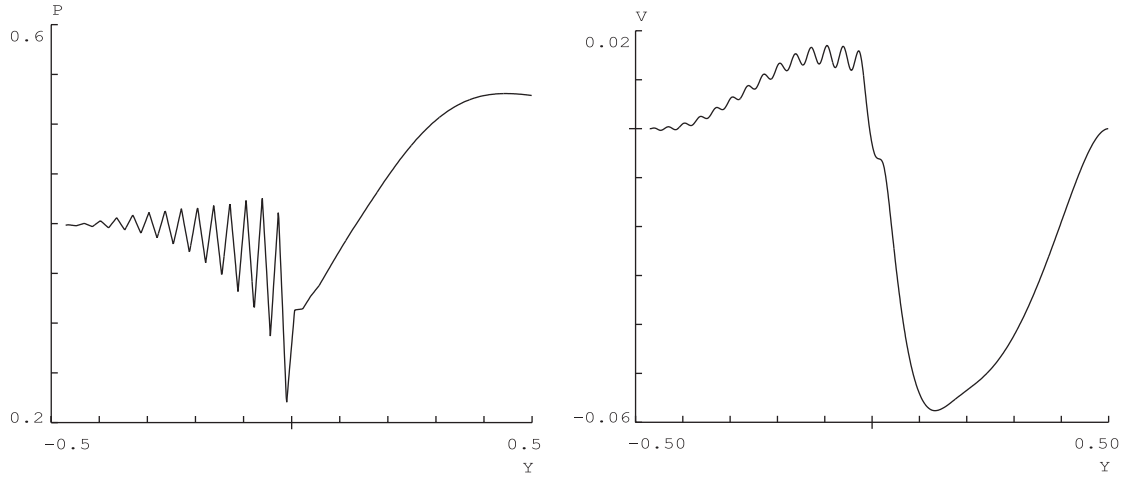

(a) (b)

Figure 20: Pressure p (a) and the velocity component v (b) exhibit oscillatory behavior in the cross section of the channel just after the back-step ($Re = 100$)

Figure 21: The channel rotated on angle α

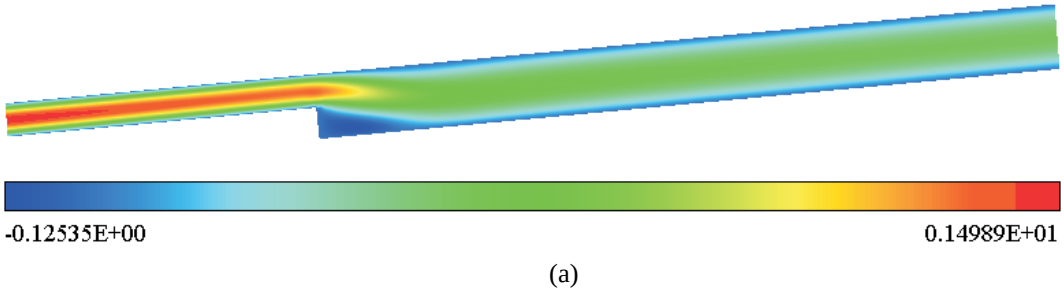

(a)

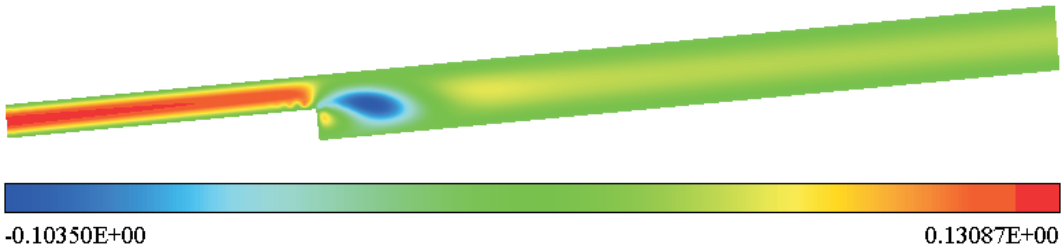

(b)

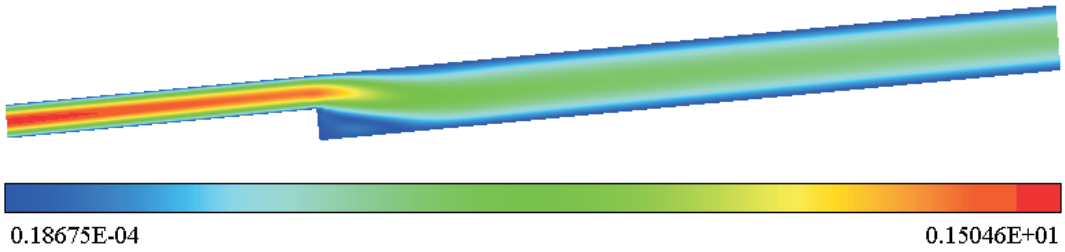

(c)

(d)

Figure 22: Distributions of: (a) u component of the velocity vector; (b) v component of the velocity vector; (c) absolute value of the velocity vector $|\mathbf{V}| = \sqrt{u^2 + v^2}$; (d) pressure p computed inside the channel shown in Figure 21 for Reynolds number of 100

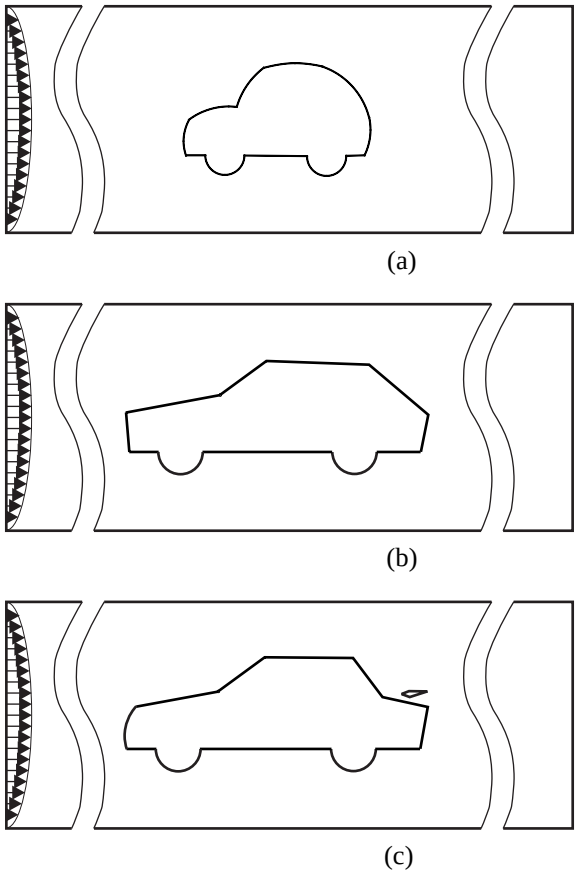

(a)

(b)

(c)

Figure 23: Cars of different shapes put in a wind tunnel

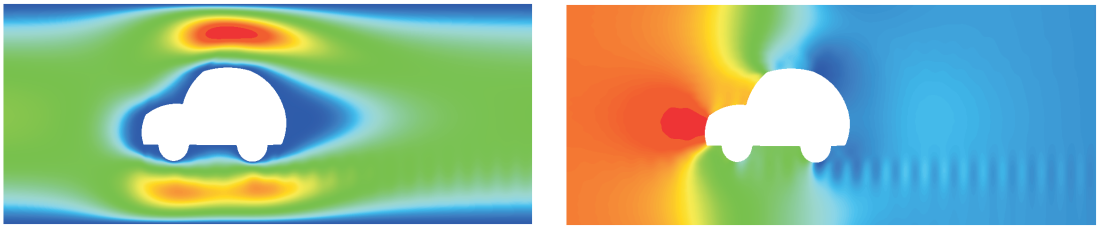

(a) (b)

Figure 24: Distribution of the components (a) u (b) pressure p around the car shown in Figure 23(a) for $Re = 100$

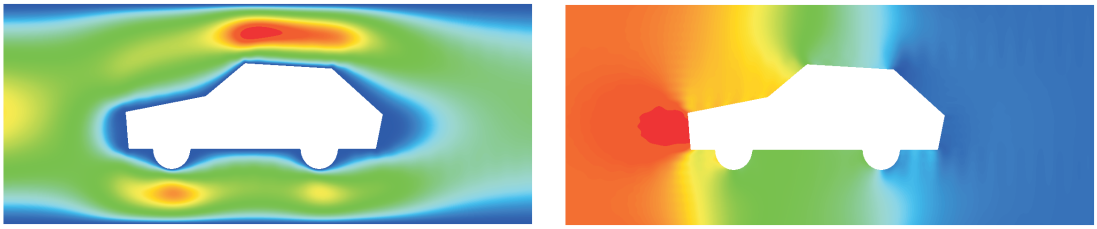

(a) (b)

Figure 25: Distribution of the components (a) u and (b) pressure p around the car shown in Figure 23(b) for $Re = 100$

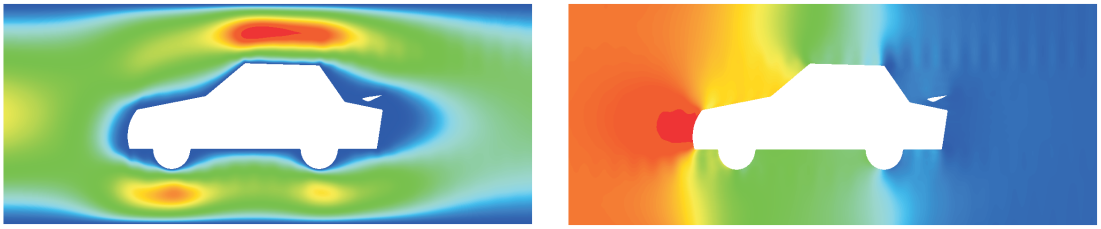

(a) (b)

Figure 26: Distribution of the components (a) u and (b) pressure p around the car shown in Figure 23(c) for $Re = 100$

[15] Mohd-Yusof J. Development of immersed boundary methods for complex geometries. Ctr annual research briefs, NASA Ames Research Center/Stanford Univ. Center for Turbulence Research, Stanford, CA, 1998.

[16] L. V. Kantorovich and V. I. Krylov. *Approximate Methods of Higher Analysis*. Interscience Publishers, 1958.

[17] Y. Krongauz and T. Belytschko. Enforcement of essential boundary conditions in meshless approximations using finite elements. *Computer Methods in Applied Mechanics and Engineering*, 131:133–145, 1996.

[18] W. K. Liu, S. Jun, S. Li, J. Adee, and T. Belytschko. Reproducing kernel particle methods for structural mechanics. *Int. J. Numer. Methods Engrg.*, 38:1655–1679, 1995.

[19] L. G. Loitsyanskiy. *Mechanics of Liquids and Gases*. Begell House, Inc., Publishers, 1995. 6th ed.

[20] Y.Y. Lu, T. Belytschko, and L. Gu. A new implementation of the element-free Galerkin. *Computer Methods in Applied Mechanics and Engineering*, 113:397–414, 1994.

[21] L. Lucy. A numerical approach to testing the fission hypothesis. *Astron. J.*, 82:1013–1024, 1977.

[22] Yu. M. Matsevity, editor. *Vladimir Logvinovich Rvachev*. Biobibliography of scientists of Ukraine. Institute for Problems in Machinery, 2001. In Russian.

[23] J. M. Melenk and I. Babuska. The partition of unity finite element method: Basic theory and applications. *Computer Methods in Applied Mechanics and Engineering*, 139:289–314, 1996.

[24] C. S. Peskin. Numerical analysis of blood flow in the heart. *J. Comp. Phys.*, 25, 1977.

[25] P. W. Randles and L. D. Libersky. Smoothed particle hydrodynamics: Some recent improvements and applications. *Computer Methods in Applied Mechanics and Engineering*, 139:375–408, 1996.

[26] V. Rvachev, T. Sheiko, V. Shapiro, and J. Uicker. Implicit function modeling of solidification in metal casting. *Transaction of ASME, Journal of Mechanical Design*, 119:466–473, December 1997.

[27] V. L. Rvachev. Analytical description of some geometric objects. *Dokl AS USSR*, 153(4):765–768, 1963.

[28] V. L. Rvachev. *Theory of R-functions and Some Applications*. Naukova Dumka, 1982. In Russian.

[29] V. L. Rvachev and T. I. Sheiko. R-functions in boundary value problems in mechanics. *Applied Mechanics Reviews*, 48(4):151–188, 1995.

[30] V. L. Rvachev, T. I. Sheiko, V. Shapiro, and I. Tsukanov. On Completeness of RFM Solution Structures. *Computational Mechanics*, 22(1), 2000.

[31] V. L. Rvachev, T. I. Sheiko, V. Shapiro, and I. Tsukanov. Transfinite interpolation over implicitly defined sets. *Computer Aided Geometric Design*, 18(4):195–220, 2001.

[32] J. A. Sethian. *Level Set Methods and Fast Marching Methods Evolving Interfaces in Computational Geometry, Fluid Mechanics, Computer Vision, and Materials Science*. Cambridge University Press, 1999. Cambridge Monograph on Applied and Computational Mathematics.

[33] J.A. Sethian. *Level Set Methods: Evolving Interfaces in Geometry, Fluid Mechanics, Computer Vision and Material Sciences*. Cambridge University Press, 1996.

[34] V. Shapiro. Theory of R-functions and applications: A primer. Tech. Report TR91-1219, Computer Science Department, Cornell University, Ithaca, NY, 1991.

[35] V. Shapiro and I. Tsukanov. Implicit functions with guaranteed differential properties. In *Fifth ACM Symposium on Solid Modeling and Applications*, Ann Arbor, MI, 1999.

[36] V. Shapiro and I. Tsukanov. Meshfree simulation of deforming domains. *Computer Aided Design*, 31:459–471, 1999.

[37] M. Stolarska, D. L. Chopp, N. Moes, and T. Belytschko. Modelling crack growth by level sets and the extended finite element method. *International Journal for Numerical Methods in Engineering*, 51(8):943–960, 2001.

[38] N. Sukumar, D. L. Chopp, N. Moes, and T. Belytschko. Modeling holes and inclusions by level sets in the extended finite element method. *Computer Methods in Applied Mechanics and Engineering*, 190(46-47):6183–6200, 2000.

[39] J. C. Tannehill, D. A. Anderson, and R. H. Pletcher. *Computational Fluid Mechanics and Heat Transfer*. Taylor & Francis, 1997. 2-nd ed.

[40] I. Tsukanov and M. Hall. Data structure and algorithms for fast automatic differentiation. *International Journal for Numerical Methods in Engineering*, 2002. Accepted for publication.

[41] I. Tsukanov and V. Shapiro. The architecture of SAGE — a meshfree system based on RFM. *Engineering with Computers*, 2002. Accepted for publication. (Available from http://sal-cnc.me.wisc.edu).

[42] Z. J. Wang. Fast nested multi-grid viscous flow solver for adaptive Cartesian /Quad grids. AIAA-96-2091, June, 1996.